Numerical investigation on natural convection of Al2O3/water nanofluid with variable properties in an annular enclosure under magnetic field

Farid Berrahil, Abdelkader Filali, Chérifa Abid, Smail Benissaad, Rachid Bessaih, Omar Matar

Numerical investigation on natural convection of Al_2O_3/Water nanofluid with variable properties in an annular enclosure under magnetic field

Farid Berrahil [1,2,*], Abdelkader Filali [3,4], Chérifa Abid [5], Smail Benissaad [2], Rachid Bessaih [2], Omar Matar [4]

[1] Science and Technology Institute, University Center Abdelhafid Boussouf, Mila, Algeria

[2] LEAP Laboratory, Department of Mechanical Engineering, Faculty of Sciences Technology, University of Frères Mentouri-Constantine 1, Constantine, Algeria

[3] Laboratoire Mécanique et système énergétique avancé, Ecole Nationale Polytechnique de Constantine, BP75, A, Nouvelle Ville Ali Mendjli, Constantine, Algeria

[4] Chemical Engineering Department, Imperial College London, South Kensington, London SW7 2AZ, UK

[5] Aix Marseille Univ, CNRS, IUSTI, Marseille, France

Corresponding author: Farid Berrahil

* E-mail: farid.berrahil@gmail.com and farid.berrahil@centre-univ-mila.dz

Abstract:

Numerical investigation of the natural convection of Al_2O_3-water nanofluid is carried out in a differentially heated vertical annulus under a uniform magnetic field. An in-house Fortran code has been developed to solve the system of equations governing the magneto-hydrodynamic flow. Computations are carried out for different Rayleigh numbers ($10^4 \leq Ra \leq 10^6$), nanoparticle diameter ($d_p = 13$ and $47\ nm$), nanoparticle volume fraction ($0 \leq \varphi \leq 0.09$), radius ratio ($2 \leq \lambda \leq 10$), and different Hartmann numbers ($0 \leq Ha \leq 100$). According to the simulation data, nanoparticle size is crucial for evaluating nanofluid properties, such as viscosity and thermal conductivity. The computational results reveal that, for nanoparticles with a diameter $d_p = 47\ nm$, the average Nusselt number $\overline{Nu_i}$ on the inner cylinder wall decreases as the nanofluid volume fraction increases. This decrease in $\overline{Nu_i}$ number is observed up to a volume fraction $\varphi = 0.05$, after which it increases again. For the full range of volumetric fractions, it is shown that increasing Ra number causes $\overline{Nu_i}$ to increase, while increasing Ha number and increasing the magnetic field causes $\overline{Nu_i}$ to decrease. Furthermore, as the Ha number increases, the heat transfer enhancement ratio En increases mainly when the magnetic field is oriented radially. Finally, new correlations of $\overline{Nu_i}$ versus Ra, φ, Ha, and λ are derived for the axial and radial magnetic fields cases.

Keywords: Natural convection, Al_2O_3-water, Lorentz forces, annulus enclosure, variable properties.

NOMENCLATURE

B_0	magnetic field, (T)
c_p	specific heat at constant pressure, $(J/kg.K)$
D	annulus gap, (m)
En	heat transfer enhancement ratio
$\boldsymbol{f}$	electromagnetic force, (N/m^3)
h	heat transfer coefficient, (W/m^2K)
J	electric current density, (A/m)
k	thermal conductivity
Nu	local Nusselt number
$\overline{Nu}$	average Nusselt number
p	pressure, (N/m^2)
P	dimensionless pressure
Pr	Prandtl number
r_i, r_o	inner and outer radii, m
Ra	Rayleigh number
t	time, (s)
T	temperature, (K)
u, w	velocities in the r and z directions, (m/s)
U, W	dimensionless velocities
r, z	cylindrical coordinates, (m)
R, Z	dimensionless cylindrical coordinates

Greek symbols

α	thermal diffusivity, (m^2/s)
β	thermal expansion coefficient, $(1/K)$
θ	dimensionless temperature
μ	dynamic viscosity
υ	kinematic viscosity, (m^2/s)
ρ	density, (kg/m^3)
σ	electrical conductivity, $(1/\Omega.m)$
τ	dimensionless time
φ	volume fraction
ψ	dimensionless stream function
ϕ	general variables
$\Delta\tau$	dimensionless time increment

Subscripts and superscripts

c	cold
EM	electromagnetic
f	base fluid
h	hot
i	inner cylinder
o	outer cylinder
p	nanoparticle
max	maximum
min	minimum
n	number of iterations
nf	nanofluid
0	reference value at cold condition

1. Introduction

Research studies related to natural convection in (a confined) cylindrical annular enclosures have received considerable attention and have remained a fundamental field to explain many physical phenomena. The application areas are compact heat exchangers, food preservation, solar collectors, nuclear reactors, and electronic cooling systems [1].

The natural convection phenomena under the applied magnetic field can be found in some experimental processes, such as cooling fusion reactors and crystal growth in liquid. Various studies in the literature have been performed to characterize natural convection and heat transfer in enclosures under applied magnetic fields. Different geometrical parameters and boundary conditions were investigated [2-13]. The magnetic field direction and strength were revealed as two major factors that significantly affected the heat transfer properties and flow patterns. Similar research studies can be found in an annular cavity under a magnetic field [14-21]. In most of these studies, the case of electrically conducting fluid characterized by a low thermal conductivity is considered.

Improvement of heat transfer performance is an essential aspect of saving energy. The low thermal properties of the working fluids, such as water, engine oil, and ethylene glycol, are critical constraints during the design of compact thermal systems with high efficiency. In contrast, Nanoparticles have been shown to have potential advantages in increasing the thermal conductivity of the base fluids. An exciting review on the nanofluid preparation methods reported by different investigators and describing the suitable method for preparing stable nanofluids has been published by Haddad et al. [22]. The final prepared nanofluid will have specific properties, i.e., thermal conductivity and dynamic viscosity, that play an essential role during heat transfer processes [23]. Choi [24] was the first who proposed the term nanofluid to designate the mixture of suspended solid nanoparticles in a base fluid. The resulting mixture is characterized by an improved effective thermal conductivity when compared to traditional fluids.

Several authors have considered examining the natural convection of nanofluids in a heated cavity with or without an applied magnetic field. Khanafer et al. [25] conducted a numerical analysis of natural convection problem in a differentially heated cavity containing a flowing nanofluid. Their results showed that $\overline{Nu}$ number is considerably increased with rising the nanoparticle volume fraction for all Grashof number values. Putra et al. [26] analyzed the natural convection inside the horizontal cylinder experimentally. Results revealed that the presence of Al_2O_3 or CuO nanoparticles in water reduced the heat transfer in which both the density and concentration of the nanoparticles played a significant role in the heat transfer deterioration. Omid Abouali and Ahmad Falahatpisheh [27] considered a vertical annulus to investigate numerically the effect of the (Al_2O_3 −water) nanofluid viscosity and particle diameters on the natural convection flow. Their results were validated first against the experimental results provided by Putra et al. [26]. A general correlation has been developed to predict the heat transfer rate for annuli, which depends on the viscosity model and particle diameter. The authors have advised that this correlation is also valid for the case of the square cavity. Ghasemi et al. [28] considered the natural convection phenomena for the case of (Al_2O_3 −water) nanofluid inside a square cavity subjected to a horizontally directed magnetic field. Their outputs showed that the computed Nu number decreases with

the augment of Ha number and increases with the extension of Ra number. However, the enhancement or deterioration of Nu number with the increased solid volume fraction depends on Ra and Ha number values. Sheikholeslami et al. [29] applied the Lattice Boltzmann method - LBM to solve the natural convection phenomena in an annulus between a cold square and a heated elliptic cylinder. Both an applied magnetic field and the influence of Brownian motion on the effective thermal conductivity were investigated. Their outputs showed that increasing Ra number and the nanoparticle volume fraction leads to an enhanced average Nu number. Increasing Ha number, on the other hand, have an opposite effect on Nu number. Later, Sheikholeslami et al. [30] analyzed the natural convection in a half-annulus enclosure exposed to a magnetic field. The applied thermal condition of one wall subjected to a constant heat flux has been considered, and various inclination angles have been texted. The results showed that rising the volume fraction of nanoparticles and Ra number improved the Nu number. In contrast, applying a magnetic field results in an inhibited flow and temperature fluctuations by decreasing the Nu number and the flow velocity. For all investigated inclination angles and low Ra numbers, increasing Ha number leads to improved heat transfer.

Computational results reported by Ashorynejad et al. [31], for the case of the horizontal cylindrical annulus, revealed that the flow fluctuations of nanofluids for a natural convection problem could be inhibited by applying an external magnetic field. In addition, the authors concluded that higher values of the average Nu number could be achieved by increasing Ra number and/or the volume fraction of nanoparticles. In contrast, increasing Ha number leads to low Nusselt number values. Sheikholeslami et al. [32] carried out numerical simulations to investigate the magneto-hydrodynamic natural convection for Al_2O_3–water nanofluid inside a horizontal annulus between a circular cylindrical enclosure and an internal heated triangular cylinder. It is found that the computed $\overline{Nu}$ number is proportional to Ra number and inversely proportional to Ha number. The authors established a new correlation of $\overline{Nu}$ number as a function of the studied physical parameters. Sheikholeslami [33] has carried out a numerical simulation on the effect of magnetic field on natural convection of nanofluid flowing inside an enclosure. An uniform temperature was imposed on the outer cylinder, while the inner cylinder was submitted to a constant heat flux. Reported results revealed that the improvement in heat transfer increases the aspect ratio and Ha number, whereas it decreases with the increasing Ra number. Mebarek-Oudina and Bessaïh [34] carried out the numerical computation of natural convection in a vertically positioned cylindrical annulus enclosure comprising Cu–water nanofluid. The case study considered the impact of two discrete heat sources having different lengths and mounted on the inner enclosure wall. Results showed that the investigated parameters, including the size and the location of the heaters, the volume fraction of nanoparticles, and Ra number, significantly affect the heat transfer characteristics. More precisely, when the heater is placed in the vicinity of the bottom wall, the heat transfer rate is improved, whereas it decreases with increasing the top or the bottom heater size. Furthermore, the heat transfer rate increases with the rising of the Ra number and the volume fraction of nanoparticles. Mebarek-Oudina et al. [35] studied

numerically the magneto-hydrodynamic natural convection in a porous vertical annular enclosure containing a nanofluid whose aspect ratio and radius ratio are equal to 2. The results revealed that the increase in heat transfer rate is proportional to the augment of Ra number, the concentration of nanoparticles, the Darcy number, and the porosity. Simultaneously, it is inversely proportional to the increase in the length of the heat source and the intensity of the magnetic field. They concluded that the improvement in heat transfer is better if Ag nanoparticles are used compared to other nanoparticles, namely, Cu, Al_2O_3 and TiO_2. Recently, Sadeghi et al. [36] conducted a numerical analysis of natural convection in an adiabatic corrugated cavity with two circular cylinders held at different temperatures using the FEM finite element method. The cavity is filled with (Fe_3O_4-water) ferrofluid. The flow is exposed to a magnetic field where the viscosity of the ferrofluid is highly dependent on its intensity. They examined the influence of various control parameters such as Ra and Ha numbers, the radiation parameter R_d, the shape aspect of the nanoparticles, the volume fraction of the ferrofluid, and the distance between the two circular cylinders on the flow behaviour and heat transfer performance. Their findings for a platelet nanoparticle shape ($m = 5.7$) suggest that the heat transfer rate and the intensity of natural convection increase monotonically with Ra and R_d but decrease at the expense of Ha. In addition, the magnetic field is more effective at low values of Ra, while thermal radiation is more effective at high values of Ra.

So far, the survey of the previous studies shows a lack of studies dealing with the effect of nanofluid properties, namely the viscosity and the thermal conductivity, and comparing those effects for the cases of axially and radially applied magnetic field. Therefore, and to the best of the author's knowledge, no detailed contributions and established correlations were provided to show those effects combined with the nanoparticle volume fraction effects, Ra and Ha numbers on the flow structure and heat transfer characteristics. Consequently, the present study aims to assess these effects numerically in a vertical cylindrical annulus containing a water-alumina. The effective thermal conductivity and viscosity of the mixture water-alumina are computed by KV (Khanafer and Vafai [37]) correlation. The influence of the parameters mentioned above is examined for two nanoparticle diameters $d_p = 13$ and $47\ nm$. It highlights that the consideration of variable fluid properties such as thermal conductivity and viscosity is of critical importance. This approach is more realistic compared to the one based on constant properties that, on the one hand, overestimate the heat transfer in hot and cold locations and the size of nanoparticles on the other.

2. Mathematical formulation

Figure 1 shows a schematic of the considered nanofluid contained between two vertical coaxial cylinders of height H and inner and outer cylinder's radius r_i and r_o, respectively. The vertical walls are differentially heated as hot inner wall (T_h) and cold outer wall (T_c) whereas the horizontal walls are kept adiabatic (thermally insulated). The annular enclosure is exposed to a constant external magnetic field, and all four walls are electrically insulated boundaries.

For an appropriate formulation of the problem, the nanofluid is supposed to be homogenous, incompressible, and Newtonian, and the flow is assumed laminar and axisymmetric. The spherical Al_2O_3 nanoparticles and the base fluid (water) are supposed in thermal equilibrium. Induced electric current, Joule heating, radiation, and viscous dissipation are neglected. In addition, the thermophysical properties of the nanoparticles and the base fluid considered in the present study are presented in Table 1 [29].

The governing equations of the nanofluid flow and heat transfer using the Boussinesq approximation are defined as follows:

$$\frac{1}{r}\frac{\partial}{\partial r}(ru)+\frac{\partial w}{\partial z}=0 \tag{1}$$

$$\rho_{nf}\left(\frac{\partial u}{\partial t}+\frac{1}{r}\frac{\partial}{\partial r}(ru^2)+\frac{\partial}{\partial z}(wu)\right)=-\frac{\partial p}{\partial r}+\left(\frac{1}{r}\frac{\partial}{\partial r}\left(\mu_{nf}r\frac{\partial u}{\partial r}\right)+\frac{\partial}{\partial z}\left(\mu_{nf}\frac{\partial u}{\partial z}\right)-\mu_{nf}\frac{u}{r^2}\right)+f_{EMr} \tag{2}$$

$$\rho_{nf}\left(\frac{\partial w}{\partial t}+\frac{1}{r}\frac{\partial}{\partial r}(ruw)+\frac{\partial}{\partial Z}(w^2)\right)=-\frac{\partial p}{\partial z}+\left(\frac{1}{r}\frac{\partial}{\partial r}\left(\mu_{nf}r\frac{\partial w}{\partial r}\right)+\frac{\partial}{\partial z}\left(\mu_{nf}\frac{\partial w}{\partial z}\right)\right)+(\rho\beta)_{nf}g(T-T_c)+f_{EMz} \tag{3}$$

$$\left(\rho c_p\right)_{nf}\left(\frac{\partial T}{\partial t}+\frac{1}{r}\frac{\partial}{\partial r}(ruT)+\frac{\partial}{\partial z}(wT)\right)=\left[\frac{1}{r}\frac{\partial}{\partial r}\left(k_{nf}r\frac{\partial T}{\partial r}\right)+\frac{\partial}{\partial z}\left(k_{nf}\frac{\partial T}{\partial z}\right)\right] \tag{4}$$

where p, T, u and w are, respectively, the dimensional pressure, temperature, and the velocity components. f_{EMr} and f_{EMz} represent the dimensional Lorenz forces in radial and axial directions, respectively, and are computed from the equation: $\boldsymbol{f_{EM}}=\sigma_{nf}[\boldsymbol{V}\times\boldsymbol{B}]\times\boldsymbol{B}$, where $\boldsymbol{B}$ and $\boldsymbol{V}$ are, respectively, the magnetic field and the velocity vectors, computed as follows:

$B=B_r$ (radial magnetic field):

$$\begin{cases} f_{EMr}=0 \\ f_{EMz}=-\sigma_{nf}\left({B_0}^2\right)w \end{cases} \tag{5a}$$

$B=B_z$ (axial magnetic field):

$$\begin{cases} f_{EMr}=-\sigma_{nf}\left({B_0}^2\right)u \\ f_{EMz}=0 \end{cases} \tag{5b}$$

The nanofluid density ρ_{nf}, thermal expansion coefficient β_{nf}, heat capacity ${c_p}_{nf}$, and thermal diffusivity α_{nf} are defined, respectively, as:

$$\rho_{nf}=(1-\varphi)\rho_f+\varphi\rho_p \tag{6}$$

$$(\rho\beta)_{nf}=(1-\varphi)(\rho\beta)_f+\varphi(\rho\beta)_p \tag{7}$$

$$\left(\rho c_p\right)_{nf}=(1-\varphi)\left(\rho c_p\right)_f+\varphi\left(\rho c_p\right)_p \tag{8}$$

$$\alpha_{nf}=k_{nf}/\left(\rho c_p\right)_{nf} \tag{9}$$

Also, the effective electrical conductivity for the used nanofluid is expressed as follows [38]:

$$\sigma_{nf}/\sigma_f = 1 + \frac{3(\sigma_p/\sigma_f - 1)\varphi}{(\sigma_p/\sigma_f + 2) - (\sigma_p/\sigma_f - 1)\varphi} \tag{10}$$

In the above equations, φ is the nanoparticle concentration in nanofluids.

The dynamic viscosity μ_{nf} and the thermal conductivity k_{nf} of nanofluids are obtained from the below respective correlations proposed by KV [37] based on the various experimental results. With this model, the properties depend on temperature, volume fraction, and particle diameter:

$$\mu_{nf}(cp) = -0.4491 + \frac{28.837}{T} + 0.574\,\varphi - 0.1634\,\varphi^2 + 23.053\frac{\varphi^2}{T^2} + 0.0132\,\varphi^3 - 2354.735\frac{\varphi}{T^3} + 23.498\frac{\varphi^2}{{d_p}^2} - 3.0185\frac{\varphi^3}{{d_p}^2} \tag{11}$$

valid in the ranges: $1\% \le \varphi \le 9\%$, $13\ nm \le d_p \le 131\ nm$ and $20^{\circ}C \le T \le 70^{\circ}C$.

$$\frac{k_{nf}}{k_f} = 0.9843 + 0.398\,\varphi^{0.7383}\left(\frac{1}{d_p(nm)}\right)^{0.2246}\left(\frac{\mu_{nf}(T)}{\mu_f(T)}\right)^{0.0235} - 3.9517\frac{\varphi}{T} + 34.034\frac{\varphi^2}{T^3} + 32.509\frac{\varphi}{T^2} \tag{12}$$

valid in the ranges: $0 \le \varphi \le 10\%$, $11\ nm \le d_p \le 150\ nm$ and $20^{\circ}C \le T \le 70^{\circ}C$.

The base fluid (water) viscosity is assumed as a temperature-dependent function defined as [39]:

$$\mu_f(T) = 2.414 \times 10^{-5} \times 10^{247.8/(T+273.15-140)} \tag{13}$$

The appropriate boundary conditions are written as follows:

$$\begin{aligned}
&\text{for} \quad r = r_o \quad \rightarrow \quad u = w = 0 \quad and \quad T = T_c \\
&\text{for} \quad r = r_i \quad \rightarrow \quad u = w = 0 \quad and \quad T = T_h \\
&\text{for} \quad z = 0 \quad \rightarrow \quad u = w = 0 \quad and \quad \partial T/\partial z = 0 \\
&\text{for} \quad z = H \quad \rightarrow \quad u = w = 0 \quad and \quad \partial T/\partial z = 0
\end{aligned} \tag{14}$$

The governing equations (1)–(5) with the applied boundary conditions are formulated in dimensionless form using the following dimensionless variables presented in equation (15):

$$\tau = t\frac{\alpha_{f_0}}{H^2}, \qquad (R,Z) = (r,z)\frac{1}{H}, \qquad (U,V) = (u,v)\frac{H}{\alpha_{f_0}}, \qquad P = \frac{pH^2}{\rho_{nf}{\alpha_{f_0}}^2}, \qquad \theta = \frac{T - T_c}{T_h - T_c} \tag{15}$$

$$\frac{1}{R}\frac{\partial}{\partial R}(RU) + \frac{\partial W}{\partial Z} = 0 \tag{16}$$

$$\frac{1}{R}\frac{\partial}{\partial R}(RU^2) + \frac{\partial}{\partial Z}(WU) = -\frac{\partial P}{\partial R} + \frac{\Pr}{(1-\varphi) + \varphi\frac{\rho_p}{\rho_f}}\left[\frac{1}{R}\frac{\partial}{\partial R}\left(\mu R\frac{\partial U}{\partial R}\right) + \frac{\partial}{\partial Z}\left(\mu\frac{\partial U}{\partial Z}\right) - \mu\frac{U}{R^2}\right] + F_{EMr} \tag{17}$$

$$\frac{1}{R}\frac{\partial}{\partial R}(RUW)+\frac{\partial}{\partial Z}(W^2)$$

$$=-\frac{\partial P}{\partial Z}+\frac{\Pr}{(1-\varphi)+\varphi\frac{\rho_p}{\rho_f}}\left[\frac{1}{R}\frac{\partial}{\partial R}\left(\mu R\frac{\partial W}{\partial R}\right)+\frac{\partial}{\partial Z}\left(\mu\frac{\partial W}{\partial Z}\right)\right]+\left((1-\varphi)+\varphi\frac{\beta_p}{\beta_f}\right)Ra\,\Pr\theta$$

$$+F_{EMz} \tag{18}$$

$$\frac{1}{R}\frac{\partial}{\partial R}(RU\theta)+\frac{\partial}{\partial Z}(W\theta)=\frac{1}{(1-\varphi)+\varphi\frac{(\rho c_p)_p}{(\rho c_p)_f}}\left[\frac{1}{R}\frac{\partial}{\partial R}\left(kR\frac{\partial\theta}{\partial R}\right)+\frac{\partial}{\partial Z}\left(k\frac{\partial\theta}{\partial Z}\right)\right] \tag{19}$$

Where:

$$\mu=\frac{\mu_{nf}}{\mu_{f_0}}\quad;\quad k=\frac{k_{nf}}{k_{f_0}} \tag{20}$$

It should be noted that for the case of a pure fluid $k=1$ and $\mu=\mu_f/\mu_{f_0}$ with μ_{f_0} is the viscosity at the reference temperature, considered equal to $22\ ^\circ C$ in the present study.

wherein equations (17) and (18), F_{EMr}, F_{EMz} are the radial and axial dimensionless Lorenz forces, respectively.

$B=B_r$:

$$\begin{cases} F_{EMr}=0 \\ F_{EMz}=-\Pr(Ha)^2\,W \end{cases} \tag{21a}$$

$B=B_z$:

$$\begin{cases} F_{EMr}=-\Pr(Ha)^2\,U \\ F_{EMz}=0 \end{cases} \tag{21b}$$

The applied boundary conditions can be formulated in dimensionless form as:

$$\begin{aligned} &\text{for} \quad R=\lambda/A(\lambda-1) \rightarrow U=W=0 \quad and \quad \theta=0 \\ &\text{for} \quad R=1/A(\lambda-1) \rightarrow U=W=0 \quad and \quad \theta=1 \\ &\text{for} \quad Z=0 \rightarrow U=W=0 \quad and \quad \partial\theta/\partial Z=0 \\ &\text{for} \quad Z=1 \rightarrow U=W=0 \quad and \quad \partial\theta/\partial Z=0 \end{aligned} \tag{22}$$

The relevant non-dimensional parameters that characterize the flow are:

Rayleigh number $Ra=\frac{g\beta_f\Delta TH^3}{\alpha_{f_0}\upsilon_{f_0}}$, Prandtl number $\Pr=\frac{\upsilon_{f_0}}{\alpha_{f_0}}$, Hartmann number $Ha=B_0H\sqrt{\frac{\sigma_f}{\mu_{f_0}}}$, the enclosure aspect ratio $A=\frac{H}{(r_o-r_i)}$, and $\lambda=\frac{r_o}{r_i}$ is the radius ratio,

To evaluate the total heat transfer rate through the enclosure, the local and the average Nusselt numbers are defined on the inner and outer cylinders as:

$$Nu=h\frac{H}{k_f}=\frac{-k_{nf}\frac{\partial T}{\partial r}}{(T_h-T_c)}\frac{H}{k_f} \tag{23}$$

Then, the local Nusselt number can be written in dimensionless form as:

$$Nu = -\left(\frac{k_{nf}}{k_f}\right)\frac{\partial\theta}{\partial R} \tag{24}$$

The average Nusselt number is defined as:

$$\overline{Nu_i} = \int_0^1 \left[-\left(\frac{k_{nf}}{k_f}\right)\frac{\partial\theta}{\partial R}\right]_{R=\frac{1}{A(\lambda-1)}} dZ \tag{25}$$

(at the inner cylinder)

$$\overline{Nu_o} = \int_0^1 \left[-\left(\frac{k_{nf}}{k_f}\right)\frac{\partial\theta}{\partial R}\right]_{R=\frac{\lambda}{A(\lambda-1)}} dZ \tag{26}$$

(at the outer cylinder)

Therefore, the heat balance of the pure fluid in the enclosure can be given as follows [40]:

$$\frac{\overline{Nu_i}}{\overline{Nu_o}} = \lambda \tag{27}$$

The meridional dimensionless stream function ψ is defined as:

$$U = \frac{1}{R}\frac{\partial\psi}{\partial Z} \quad , \quad W = -\frac{1}{R}\frac{\partial\psi}{\partial R} \tag{28}$$

The enhancement of heat transfer ratio between the pure fluid and the nanofluid ($\varphi = 0.09$) is defined by:

$$En = \frac{\overline{Nu_i}(\varphi = 0.09) - \overline{Nu_i}(base\ fluid)}{\overline{Nu_i}(base\ fluid)} \times 100 \tag{29}$$

3. Numerical details and model verification

The governing equations presented in section 2 are solved by the control volume-based discretization method (Patankar [41]). The pressure and velocity of Eqs. (1) – (4) are coupled using the SIMPLER algorithm. A fully implicit first-order forward Euler scheme is used for temporal discretization. The second-order central finite difference schemes spatially discretize the governing equations, then, the discretized equations for each variable are solved using the tri-diagonal matrix algorithm (TDMA).

Grid sensitivity tests are performed, allowing the best grid's characterization to reduce computational time with a high degree of accuracy. The different uniform grid sizes are tested from 52×52 to 202×202 for $Ra = 10^5$, Pr = 6.2, $Ha = 50$ (radial magnetic field), $\varphi = 0.06$ and $d_p = 13\ nm$. Table 2 illustrates the effect of the different tested grids on the average Nu number of the inner cylinder, the maximum velocities, and the maximum stream function. The grid independence tests indicated that a grid size of 102×102 ensures the best compromise between computational effort and required accuracy. The selected convergence criterion for the performed computations is:

$$\left|\frac{\phi^n - \phi^{n-1}}{\phi^n}\right| < \varepsilon = 10^{-5} \tag{30}$$

In the above equation, ϕ represents the different computed variables U, W or θ and the n represents the iteration number.

The current computational results are compared with those available in the literature to validate the accuracy of the present modeling. A first validation is carried out with the results of Choukairy et al. [40] for the case of natural convection ($\mathrm{Pr} = 0.7$) in an annular cavity differentially heated for different radii ratios. It should be noted that in the case of a square cavity ($A = 1$), the radii ratio tends to 1 ($\lambda \to 1$). The results reported in figure 4 show an excellent agreement. The second validation is performed against the results of Sankar et al. [14] for the case of magneto-hydrodynamic natural convection in enclosures. A similar configuration was analyzed for the case of the applied magnetic field and a low Prandtl number ($\mathrm{Pr} = 0.054$) for $A = 1$ and $\lambda = 2$. Two cases corresponding to $Ra = 10^4$ and $Ha = 40$ (radial magnetic field) and $Ra = 10^6$ and $Ha = 100$ (axial magnetic field) are considered. As presented in figure 4 in the form of isotherms and stream functions, the obtained results are in good agreement with those of Sankar et al. [14].

Final numerical validation was carried out for the case of the MHD natural convection of a nanofluid (CuO - water) within a square enclosure that is differentially heated. The models of Brinkman [42] and Maxwell-Garnett [43] are used respectively to determine the nanofluid's dynamic viscosity and thermal conductivity. Table (3) demonstrates the quantitative comparison of the present work with those computed by Ghasemi et al. [28] with a difference of less than 0.02%. Results presented in figure 4 show a perfect agreement between the present isotherms and streamlines with those presented in reference [28]. This allows us to confirm that the developed FORTRAN code is validated successfully, and it can accurately solve the flow field and temperature variation in the cavity.

4. Results and discussion

The consequence of adding Al_2O_3 nanoparticles of different diameters ($d_p = 13$ and $47\ nm$) in the base fluid on the isotherms and streamlines for various Rayleigh numbers $Ra = 10^4$, 10^5 and 10^6 is illustrated in figure 5. This figure ~~obviously~~ shows the effect of increasing Ra number on the nanofluid flow ($\varphi = 0.09$) and the pure water ($\varphi = 0$) with the important effect of the nanoparticle's diameter on the flow structure and the thermal field.

For the streamlines, there are significant variations in the central region, notably for high values of Ra number ($Ra \geq 10^5$) for both cases of diameters. The addition of nanoparticles of small diameter ($d_p = 13\ nm$) increases the strength of the streamlines, particularly in the central region. Unlike the case of $d_p = 47\ nm$, the weakening of the flow intensity is noted relative to the flow of the base fluid. However, near the isothermal walls and small Rayleigh number values, the stream function magnitude variation is minor.

Comparatively significant variations in the central region and near the upper and lower walls for high Rayleigh number values could be observed for isotherms. The heat transfer near the isothermal walls of the small nanoparticle nanofluid is slightly higher than that of pure water. However, the difference increases with increasing Rayleigh number, suggesting an improved heat transfer when the working fluid is the nanofluid. On the other hand, the opposite situation is happening for the nanofluid with large nanoparticles, and therefore, the most important heat transfer occurs in water. Thus, the

isotherms for $d_p = 13\ nm$ are more distorted compared to the case of $d_p = 47\ nm$. For a better understanding of these results, the thermo-physical properties, namely viscosity, and conductivity are strongly linked to the temperature, the volume fraction, and the nanoparticle's diameter. To better understand these results, the thermo-physical properties, namely viscosity and conductivity, are strongly linked to the temperature, volume fraction, and nanoparticle's diameter. The increase in temperature leads to a decreased dimensionless viscosity. Also, this decrease is more pronounced for smaller nanoparticle's diameters. Indeed, the impact of the high viscosity of the nanofluid for $d_p = 47\ nm$ is complemented by an increased heat transfer anticipated by the nanoparticle's elevated thermal conductivity, although this improvement is minor compared to the drop favored by the viscosity. This behavior leads to the nanofluid flow's intensification, whose diameter is smaller than the base fluid flow and deceleration of the nanofluid flow whose diameter is larger (see the maximum stream function). This behavior leads to the nanofluid flow's intensification, whose diameter of the nanoparticles is smaller than the base fluid flow and deceleration of the nanofluid flow whose diameter of the nanoparticles is larger (see the maximum stream function).

Figure 6 presents the variation of the local Nu number along the surface of the inner (hot) and outer (cold) cylinders at various Rayleigh numbers for $\varphi = 0{,}09$ and $d_p = 13$ and $47\ nm$. In all cases, the local Nu number near the hot wall rises to a maximum local value at the bottom and subsequently declines along with the inner cylinder to a minimum value at the top. However, the opposite effect occurs with a different magnitude order for the local Nu number near the cold wall due to the curvature effect. However, for the local Nu number near the cold wall, the opposite effect occurs with a different magnitude order due to the curvature effect. It should be noted that the maximum heat transfer rate near the isothermal walls is mostly due to the distribution of the maximum axial velocity, which characterizes, on the one hand, the upward or downward movement of the nanofluid and on the other hand, the presence of a large radial temperature gradient in these regions. In the case of $d_p = 47\ nm$, it is remarkable that an increase in the nanoparticles volume fraction ($\varphi = 0.09$) indicates a declined local Nu number compared to that of pure water. On the other hand, for $d_p = 13\ nm$, an increase in the Nu number is observed. This result can be explained through Figure 7, which shows the axial velocity and temperature profiles as a function of the radius R at mid-height of the enclosure for various Ra numbers and for $\varphi = 0$ and $0{,}09$ ($d_p = 13$ and $47\ nm$). In addition, the axial velocity exhibits a parabolic variation in the vicinity of the isothermal walls due to the presence of the buoyancy force in the enclosure. The axial velocity and temperature profiles are very sensitive between the base fluid and the nanofluid and the nanoparticles' diameters. This is caused by the changed nanofluid conductivity and viscosity where the formulas (Eqs. 11 and 12) are simply sensitive to the volume fraction, the temperature, and the nanoparticle's diameter. However, the axial velocity of the nanofluid for $d_p = 13\ nm$ is higher than that of pure fluid in the vicinity of the hot region and lower on the cold part. For $d_p = 47\ nm$, the axial velocity is lower

than that of the base fluid on both sides. This means that the suspension and the nanoparticles' diameter affect the flow field in which the velocity tends to zero around the center of the cavity. This area widens as the Rayleigh number increases. The axial velocity profiles also give an idea of the flow rotation direction. Regarding the temperature profiles, the temperature gradients for the particles of diameter $d_p = 47\ nm$ are more important near the isothermal walls compared to the case of $d_p = 13\ nm$ and to the base fluid. On the other side, the temperature of the case $d_p = 13\ nm$ is higher than the case $d_p = 47\ nm$ and the base fluid far from the walls for the values of $Ra \geq 10^5$. We can relate this result to the distribution of the conductivity and dimensionless viscosity in these regions.

To shed more light on our results and highlight what we have found in the present study compared to previously published data, Table (4) presents an overview of some previously published works for natural convection of nanofluids in cylinder/annulus enclosure with and without applied magnetic field. Details of the used methods, models, type of nanofluids and the range of the investigated parameters are also provided. In general, the present results agree well with previous findings from various investigations and the discussion on the compared results for the different investigated parameters are reported trough the following texts. Figure 8 presents the computed average Nu number against the volume fraction of the nanoparticles for various Ra number values, for $Ha = 0$ and $d_p = 13$ and $47\ nm$. First, it is observed that the convection becomes more pronounced with increasing Ra number, and therefore an increased average Nu number. In the absence of the magnetic field, and for all Ra number values, the average Nu number rises slightly as the nanoparticles' volume fraction increases from 0 to 1%. This is due to the nanoparticles' presence with a low concentration, which does not affect the nanofluid's viscosity. Similar observation has been reported by Abu-Nada et al. [44].

In the case of $d_p = 47\ nm$, it is observed that an increase of the volume fraction of nanoparticles leads to a declined average Nu number. On the other hand, for $d_p = 13\ nm$, it is observed that, for a low concentration of nanoparticles (volume fraction < 5%), a decrease in the average Nu number occurs to a minimum value. However, this trend is inversed for higher concentration (volume fraction > 5%) where an increase in the average Nu number was observed. Generally, the consideration of nanoparticles in the base fluid has two opposite effects on the computed heat transfer rate: a positive and desirable effect motivated by the existence of nanoparticles characterized by high thermal conductivity and a negative, undesirable effect favoured by the increased fluid viscosity caused by the presence of nanoparticles. Thus, nanoparticles with large diameters will produce a high viscous nanofluid, which will reduce the intensity of convection and consequently decrease the average Nu number. However, the consideration of nanoparticles with small diameters will produce a less viscous nanofluid, which will improve the convection mechanism. This behavior is also observed in the numerical results of Arani et al. [49] which indicate a strong dependence of the mean Nusselt number on the diameter of the nanoparticles d_p where the mean Nusselt number is a decreasing function at a range of d_p between 30 and 90 nm.

In addition, the improvement in the heat transfer of the nanofluid ($\varphi = 0.09$) in comparison with the base fluid is more noticeable for an increased Rayleigh number (20.49% for $Ra = 10^6$, 18.29% for $Ra = 10^5$ and 15.37% for $Ra = 10^4$), while deterioration is observed for $d_p = 47\ nm$. Referring to Table (4), our results agree well with the findings reported by the experimental study of Putra [26] and the numerical study of Omid Abouali and Ahmad Falahatpisheh [27] concerning large particles $d_p = 131.2\ nm$ and $36\ nm$, respectively. In fact, the improvement in heat transfer was influenced in the opposite way where detorioration took place with increasing volume fraction of nanoparticles.

Figure 9 describes the impact of the radius ratio on flow and thermal behavior. Two radius ratios $\lambda = 4$ and 10 are considered for two values of Rayleigh number $Ra = 10^5$ and 10^6 and for different volume fractions φ. It is observed that the rising radius ratio leads to a slight modification in the flow structure. Thus, for different volume fractions, the flow for $Ra = 10^5$ is composed of a single primary cell that occupies the entire enclosure, and the centre of this cell moves towards the wall of the outer cylinder. This result is mainly due to the curvature, which destroys the centro-symmetrical properties of the flow and computes the temperature field noted in the rectangular enclosure case ($\lambda = 1$). Moreover, the flow's weakening is remarkable with the increase of $\varphi = 0.03$ and 0.06 compared to the base fluid flow. The reduction in the values of $|\psi|_{max}$ illustrates this attitude through Figure 10, which shows the distribution of the maximum stream function as a function of the radius ratio for different volume fractions. This behavior can be explained by the dominance of nanofluid viscosity's unfavourable effect over the favourable effect of thermal conductivity, which causes this deceleration of nanofluid flow. A different result is obtained for $\varphi = 0.09$ where the nanofluid flow intensity is important compared to the base fluid flow. Indeed, the influence of the high thermal conductivity of the flowing nanofluid improves the circulation driven by the buoyancy versus viscosity forces. This figure also clearly indicates that the intensity of the flow decreases with increasing the radius ratio λ. As Ra increases to 10^6, this leads to a spread of the main cell in the radial direction and the presence of two secondary cells of different sizes within this cell. The same result is obtained regarding the weakening of the flow with the increase from φ to 0.06 and the flow's intensification to φ = 0.09 compared to the base fluid flow.

Regarding the thermal field, the increase in the radius ratio leads to an increased density of the isothermal lines in the vicinity of the hot internal wall, indicating a strong temperature gradient. However, the opposite behaviour occurs in the vicinity of the cold external wall, where the temperature gradient is very low. Therefore, this effect leads to the reduction of the temperature in the chamber core. This result agrees well with Satya Sai et al. [53] and Woon Shing Yeung [54]. In the presence of the nanoparticles, it is evident that by enhancing the volume fraction of the flowing nanoparticles, the isotherms become less distorted than the pure fluid case and show an almost similar tendency as they approach the hot wall and move away from the hot wall to the cold wall.

For a better analysis of the radius ratio effect on the heat transfer in the annular enclosure, the average Nu number is presented in Figure 11 for three Rayleigh number values and four values of the radius ratios. First, it is revealed that the rate of heat transfer is improved as the Rayleigh number increases. The increasing radius ratio results in a declined thickness of the thermal boundary layer at the inner cylinder's hot wall. Reducing this layer causes temperature gradients to increase, which tends to increase the Nu number accordingly. Generally, the average Nu number's variation against the volume fraction presents a similar appearance to that observed in Figure 7. Therefore, the same reasoning is also applied regarding the behaviour of the average Nu versus the volume fraction for $\lambda = 4$, but for $\lambda \geq 6$ the results revealed that, Nu number is higher than that of pure fluid for all volume fractions. In such a case, the effect of increased thermal conductivity is more pronounced and predominates over the impact of increased viscosity, especially for a high-volume fraction.

The heat transfer enhancement ratio "En" caused by the introduced nanoparticles ($\varphi = 0.09$) is presented in Figure 12 for several values of Ra and λ. The results show that the ratio En evolves in a monotonically increasing way when the radius ratio rises. In parallel, this figure also indicates that increasing Ra number causes an increased heat transfer enhancement ratio due to a strong convective heat transfer effect.

The effect of the orientation and strength of the magnetic field on the streamlines and isotherms are shown in Figure 13 for $Ra = 10^6$, $\varphi = 0.09$, $d_p = 13$ and $47\ nm$. The flow is characterized by the primary cell with two secondary cells located at mid-height near the inner and outer cylinders for no applied magnetic field case. The application of the radial magnetic field causes noticeable changes in the flow field. Once the magnetic field's strength increases, the flow becomes a single cell with a significant concentration of streamlines at the top of the enclosure caused by the axial Lorentz force's action. Smaller changes in the flow structure are observed for the two cases $d_p = 13$ et $47\ nm$. It is interesting for the axially oriented magnetic field to note two secondary cells inside the primary cell with a concentration of streamlines at the isothermal walls. This phenomenon can be interpreted as the consequence of the action of the resulting Lorentz radial force. Moreover, it can be observed that the centers of these secondary vortices continue to move downward in the vicinity of the hot wall and upward in the vicinity of the cold wall due to the increased magnetic field strength of a side and on the other side, the effect of the curvature of the annular enclosure.

Table 5 shows the flow characteristics such as the maximum radial and axial velocities and the maximum stream function for $\varphi = 0.09$, $d_p = 13\ nm$ and for different numbers of Ha and Gr. Usually, when the magnetic field strength rises, the annulus' flow movement is damped, and the maximum stream function value decreases significantly. Additionally, this decrease is more significant when the magnetic field is oriented radially. However, the rates of decline are different for different Rayleigh numbers. For example, for the Rayleigh numbers of $Ra = 10^4$, 10^5 and 10^6, if we vary $Ha = 0$ to 25, the maximum stream function values decline respectively by 32.4%, 61.7%, and 79.3% for a radial magnetic field

and 32.1%, 62.3%, and 89.6% for an axial magnetic field. Similarly, Ashorynejad et al. [31] and Sheikholeslami et al. [32] had already observed this decrease in $|\psi_{nf}|_{max}$ as Ha increases. Hence, the trend indicates that the magnetic field's influence on fluid flow increases when the Rayleigh number is increased.

Regarding the thermal field, conduction is more pronounced compared to convection for intense magnetic fields. The isotherms become less and less deformed, especially near isothermal walls when the magnetic field is oriented radially. However, at the heart of the annular space, these isotherms are parallel and inclined concerning the case $Ha = 0$, where the lines are aligned horizontally. For the case of the axially oriented magnetic field, the isotherms' straightening and alignment are noticed in the vicinity of the isothermal walls and likewise close to the heart of the annular space with a very significant inclination.

Figure 14 presents the computed average Nu number versus Hartmann number for $Ra = 10^6$, $\varphi = 0, 0.03, 0.06$ and 0.09, $d_p = 13$ and $47\ nm$ and for two orientations of the radial and axial magnetic field. Based on the results of [29,31,32,33] indicating the effect of the magnetic field on the heat transfer which is accompanied in all cases by a decrease in the average Nu number with the increase of Ha. This result is due to the flow's deceleration (see Table 5) by the Lorentz force's effect, which acts in the opposite flow direction. Thus, reducing the flow velocity induces an enhanced thickness of the thermal boundary layer. This layer's evolution produces a diminishing temperature gradient at the heated wall, leading to a decreased Nu number.

The magnetic field orientation has also been observed and is more pronounced in the radial direction. This is because the resulting axial Lorentz force significantly damps the motion of the flow induced by the buoyancy force. This force becomes stronger with strong magnetic fields. The effect of nanoparticle diameter is most evident at an intense magnetic field where the curves of $\overline{Nu}_i$ at a different volume fractions become tighter for $d_p = 47\ nm$. On the other hand, for $d_p = 13\ nm$, the difference is relatively large. This difference can be attributed to the effect of high viscosity for the large diameter of the nanoparticles. For $Ra = 10^4$, the effect of the magnetic field orientation on the variation of the Nu number is insignificant because of the impact of convection, which is relatively weak on the one hand and the dominance of the conduction regime on the other hand from $Ha = 50$. Furthermore, this variation of $\overline{Nu}_i$ decreases with increasing the strength of the magnetic field before reaching an asymptotic value. The increased volume fraction of the nanoparticles results in a further increase in this asymptotic value. At high values of the Hartmann number, conduction is dominant, and the effective thermal conductivity of the nanofluid contributes to an enhanced Nu number relative to those of the pure fluid in all cases. However, for high Rayleigh numbers, say at $Ra = 10^6$, the Nu number for the pure fluid is relatively higher than that of a nanofluid for $d_p = 47\ nm$ and $\varphi = 0.09$, which results in the detrimental effect of the viscosity, which counterbalanced the favourable impact of thermal conductivity on one side and the other side the weak effect of the magnetic field axial direction compared to that of the radial direction.

Figure 15 shows the impact of Hartmann number Ha and the radius ratio λ on the computed average Nu number for $Ra = 10^6$ and $\varphi = 0.09$ for both radial and axial magnetic field directions. Once the strength of the magnetic field increases, then $\overline{Nu_i}$ decreases due to the dominance of conduction. This figure also reveals that the decrease in the $\overline{Nu_i}$ is relatively large when the magnetic field is directed radially for all the ratios λ. Moreover, the rate of decrease of the average Nusselt number $(\overline{Nu_i}(Ha = 0) - \overline{Nu_i}(Ha = 100)/\overline{Nu_i}(Ha = 0))$ is even stronger when the radius ratio decreases. For example, in the case of a radial magnetic field, the rate of decrease of $\overline{Nu_i}$ for $\lambda = 2$ when Ha varies from 0 to 100 is 57.25%, while for $\lambda = 10$, the rate of decrease is 52.28 % but for the case axially applied magnetic field, the decrease rates for $\lambda = 2$ and 10 are respectively 41.78% and 30.27%.

From the above-achieved results, it is evident that the average Nu number can be correlated as a function of Ra and Ha numbers, the volume fraction φ, and the radius ratio λ as $\overline{Nu_i} = f(Ra, \varphi, Ha, \lambda)$. Two original developed correlations provided in equations (31) and (32) are proposed and derived for the radial and axial magnetic fields cases. The coefficients are obtained using the least square regressions method in which R^2 of 0.983 and 0.978 are obtained for the radial and axial magnetic fields cases, respectively. It is essential to mention that these two correlations correspond to the case of small nanoparticles diameter $d_p = 13\,nm$ in which an important heat transfer enhancement is obtained. Furthermore, the derived correlations are valid within the range of the investigated parameters of the present study. Within these limits, the correlations can accurately capture the overall variation of the average Nu number. These derived correlations are:

- For the radial magnetic field, B_r:

$$\overline{Nu_i} = 39.935 - 19.618Ra^* - 7.699\varphi^* + 1.378Ha^* + 0.611\lambda^* + 1.174Ra^*\varphi^* - 0.439Ra^*Ha^* + 1.877Ra^*\lambda^* - 0.038\varphi^*Ha^* + 1.966\varphi^*\lambda^* - 0.275Ha^*\lambda^* + 2.516(Ra^*)^2 + 3.339(\varphi^*)^2 + 0.036(Ha^*)^2 - 3.153(\lambda^*)^2 \quad (31)$$

- For the axial magnetic field, B_z:

$$\overline{Nu_i} = 59.07 - 27.15Ra^* - 9.897\varphi^* + 0.697Ha^* - 2.669\lambda^* + 1.165Ra^*\varphi^* - 0.244Ra^*Ha^* + 2.727Ra^*\lambda^* - 0.023\varphi^*Ha^* + 2.041\varphi^*\lambda^* - 0.157Ha^*\lambda^* + 3.235(Ra^*)^2 + 5.684(\varphi^*)^2 + 0.011(Ha^*)^2 - 3.797(\lambda^*)^2 \quad (32)$$

In the above correlations, $Ra^* = \log(Ra)$, $Ha^* = 0.1Ha$, $\lambda^* = 0.1\lambda$ and $\varphi^* = 10\varphi$.

The heat transfer enhancement ratio "En" computed for the case of existing nanoparticles ($\varphi = 0.09$) for various Ha and Ra values is presented in Figure 16. When the magnetic field is absent, it is observed that the effect of adding nanoparticles is more evident at high Ra number values compared to the case of low Ra number. However, an inverse behavior is noticed when the magnetic field is applied. For $Ha = 0$, the enhancement ratio increases with increasing Ra number. As explained previously, this result is due to the increased convection mechanism. However, for high values of Ha, this ratio increases with the decrease of Ra number due to the dominant conduction in the heat transfer mechanism. Thus, the consideration of nanoparticles with high thermal conductivity results in an enhanced conduction process and improves

the heat transfer enhancement ratio as demonstrated by the numerical work of Sheikholeslami et al. [29.33] indicating that En is an increasing function with Ha. For high Ra number values, the strong magnetic field effectively reduces convective motion, and consequently, the conduction becomes the prevalent mechanism; hence, the enhancement ratio increases. The magnetic field orientation's influence has also been observed. Most interestingly, the magnetic field is more effective when directed radially, which results in the high values of En in this case compared to the axial magnetic field.

Conclusion

In the present study, the finite volume method-FVM is used to solve the system of equations governing the flow and heat transfer by natural convection in differentially heated vertical annulus subject to an uniform magnetic field, oriented in the axial and radial directions. The Al_2O_3-water nanofluid is used, and the flow field and heat transfer results have been presented in the form of streamlines, isotherms, and Nusselt number. Several combinations of parameters in the range of Rayleigh number $10^4 \leq Ra \leq 10^6$, Hartmann number $0 \leq Ha \leq 100$, nanoparticle volume fraction $0 \leq \varphi \leq 0.09$, radius ratio $2 \leq \lambda \leq 10$, and nanoparticle diameter $d_p = 13$ and $47\ nm$ have been considered.

A detailed validation of the numerical model was carried out, and the main conclusions that can be drawn from this study can be summarized as follows:

- In the absence of a magnetic field, increasing the Rayleigh number improves the average Nusselt number over the full range of the parameter set combinations. On the other side and for an applied magnetic field, the average Nu number decreases with the increasing of the Hartmann number.
- For radius ratio $\lambda = 2$, increment of the volume fraction of nanoparticles led to the continuous deterioration of the average Nu number at $d_p = 47\ nm$, however, for $d_p = 13\ nm$, the average Nu number decreases to a minimum value at $\varphi = 0.05$, then it increases to reach its maximum value at $\varphi = 0.09$. This behaviour of the average Nu number for $d_p = 13\ nm$ remains the same for $\lambda = 4$. However, for $\lambda \geq 6$, the average Nu number is greater than that of pure fluid for all volume fractions. In this case, the effect of increased thermal conductivity is more pronounced and predominates over the impact of increased viscosity, especially for a high-volume fraction.
- The influence of the magnetic field is more pronounced in the radial direction. This is because the resulting axial Lorentz force significantly damps the motion of the flow induced by the buoyancy force. This force becomes greater for strong magnetic fields.
- The rate of decrease in the average Nu number caused by the application of the magnetic field is greater as the radius ratio λ decreases.

- As the Rayleigh number and the radius ratio λ are increased, the heat transfer enhancement ratio En increases with the insertion of nanoparticles ($\varphi = 0.09$) of small diameters.
- The heat transfer enhancement ratio En increases as the Hartmann number is increased, and for high values of Ha, this ratio increases further at the expense of the Rayleigh number.

References

[1] S. Ostrach, Natural convection in enclosures, Journal of Heat Transfer 110 (1998) 1175–1190.

[2] J.P. Garandet, T. Albussoiere, R. Moreau, Buoyancy driven convection in a rectangular enclosure with a transverse magnetic field, International Journal of Heat and Mass Transfer 35 (1992) 741–748.

[3] S. Alchaar, P. Vasseur, E. Bilgen, Natural convection heat transfer in a rectangular enclosure with a transverse magnetic field, Journal of Heat Transfer 117 (1995) 668–673.

[4] N.M. Al-Najem, K.M. Khanafer, M.M. El-Refaee, Numerical study of laminar natural convection in tilted enclosure with transverse magnetic field, International Journal of Numerical Methods for Heat and Fluid Flow 8 (6) (1998) 651–672.

[5] A.Y. Gelfgat, P.Z. Bar-Yoseph, The effect of an external magnetic field on oscillatory instability of convective flows in a rectangular cavity, Physics of Fluids 13 (8) (2001) 2269–2278.

[6] M.A. Hossain, M.Z. Hafiz, D.A.S. Rees, Buoyancy and thermo capillary driven convection flow of an electrically conducting fluid in an enclosure with heat generation, International Journal of Thermal Sciences 44 (7) (2005) 676–684.

[7] I. E. Sarris, S. C. Kakarantzas, A. P. Grecos, N. S. Vlachos, MHD natural convection in a laterally and volumetrically heated square cavity, International Journal of Heat and Mass Transfer 48 (16) (2005), 3443–3453.

[8] M.C. Ece, E. Büyük, Natural-convection flow under a magnetic field in an inclined rectangular enclosure heated and cooled on adjacent walls, Fluid Dynamics Research 38 (8) (2006) 564–590.

[9] N. A. Pelekasis, Linear stability analysis and dynamic simulations of free convection in a differentially heated cavity in the presence of a horizontal magnetic field and a uniform heat source, Physics of Fluids 18 (3) (2006) 1–23.

[10] M. Sathiyamoorthy, A. Chamkha, Effect of magnetic field on natural convection flow in a liquid gallium filled square cavity for linearly heated side wall(s), International Journal of Thermal Sciences 49 (9) (2010) 1856–1865.

[11] M.N. Kherief, K. Talbi, F. Berrahil, Effects of inclination and magnetic field on natural convection flow induced by a vertical temperature, Journal of Applied Fluid Mechanics 5 (1) (2012) 113–120.

[12] F. Berrahil, S. Benissaad, C. Abid, M. Médale, Natural convection with volumetric heat generation and external magnetic field in differentially heated enclosure, Proceedings of the Institution of Mechanical Engineers, Part C: Journal of Mechanical Engineering Science 228 (15) (2014) 2711–2727.

[13] M.N. Kherief, F. Berrahil, K. Talbi, Magneto-hydrodynamic flow in a two-dimensional inclined rectangular enclosure heated and cooled on adjacent walls, Journal of Applied Fluid Mechanics 9 (1) (2016) 205–213.

[14] M. Sankar, M. Venkatachalappa , I.S. Shivakumara, Effect of magnetic field on natural convection in a vertical cylindrical annulus, International Journal of Engineering Science 44 (20) (2006) 1556–1570.

[15] M. Sankar, M. Venkatachalappa, Younghae Do, Effect of magnetic field on the buoyancy and thermocapillary driven convection of an electrically conducting fluid in an annular enclosure, International Journal of Heat and Fluid Flow 32 (2) (2011) 402–412.

[16] S.C. Kakarantzas, I.E. Sarris, N.S. Vlachos, Natural convection of liquid metal in a vertical annulus with lateral and volumetric heating in the presence of a horizontal magnetic field, International Journal of Heat and Mass Transfer 54 (15,16) (2011) 3347–3356.

[17] M. Afrand, S. Rostami, M. Akbari, S. Wongwises, M. H. Esfe, A. Karimipour, Effect of induced electric field on magneto-natural convection in a vertical cylindrical annulus filled with liquid potassium, International Journal of Heat and Mass Transfer 90 (2015) 418–426.

[18] F. Mebarek-Oudina, R. Bessaih, Oscillatory magneto-hydrodynamic natural convection of liquid Metal between vertical coaxial cylinders, Journal of Applied Fluid Mechanics 9 (4) (2016) 1655–1665.

[19] S.C. Kakarantzas, L.Th. Benos, I.E. Sarris, B. Knaepen, A.P. Grecos, N.S. Vlachos, MHD liquid metal flow and heat transfer between vertical coaxial cylinders under horizontal magnetic field, International Journal of Heat and Fluid Flow 65 (2017) 342–351.

[20] M. Afrand, Using a magnetic field to reduce natural convection in a vertical cylindrical annulus, International Journal of Thermal Sciences 118 (2017) 12–23.

[21] M. Afrand, D. Toghraie, A. Karimipour, S. Wongwises, A numerical study of natural convection in a vertical annulus filled with gallium in the presence of magnetic field, Journal of Magnetism and Magnetic Materials 430 (2017) 22–28.

[22] Z. Haddad, C. Abid, H. F. Oztop, A. Mataoui. A review on how the researchers prepare their nanofluids. International Journal of Thermal Sciences 76 (2014) 168-189.

[23] Z. Haddad, C. Abid, A. A. Mohamad, O. Rahli, S. Bawazer. Natural convection of silica–water nanofluids based on experimental measured thermophysical properties: critical analysis. Heat Mass Transfer 52 (2016) 1649–1663.

[24] S.U.S Choi, Enhancing thermal conductivity of fluids with nanoparticles, in: D.A. Siginer, H.P. Wang (Eds.), Developments and Applications of Non-Newtonian Flows, ASME, New York, Vol. 66, 1995, pp. 99–105.

[25] K. Khanafer, K. Vafai, M. Lightstone, Buoyancy-driven heat transfer enhancement in a two-dimensional enclosure utilizing nanofluids, International Journal of Heat and Mass Transfer 46 (19) (2003) 3639–3653.

[26] N. Putra, W. Roetzel, and S. K. Das, Natural convection of nanofluids, Heat and Mass Transfer 39 (2003) 775–784.

[27] O. Abouali, A. Falahatpisheh, Numerical investigation of natural convection of Al_2O_3 nanofluid in vertical annuli, Heat and Mass Transfer 46 (2009) 15–23.

[28] B. Ghasemi, S.M. Aminossadati, A. Raisi, Magnetic field effect on natural convection in a nanofluid-filled square enclosure, International Journal of Thermal Sciences 50 (9) (2011), 1748–1756.

[29] M. Sheikholeslami, M. Gorji-Bandpy, D.D. Ganji, Numerical investigation of MHD effects on Al_2O_3 water nanofluid flow and heat transfer in a semi-annulus enclosure using LBM, Energy 60 (2013) 501–510.

[30] M. Sheikholeslami, M. Gorji-Bandpy, D.D. Ganji, Soheil Soleimani, Effect of a magnetic field on natural convection in an inclined half-annulus enclosure filled with Cu–water nanofluid using CVFEM, Advanced Powder Technology 24 (2013) 980–991.

[31] H. R. Ashorynejad, A. A. Mohamad, M. Sheikholeslami, Magnetic field effects on natural convection flow of a nanofluid in a horizontal cylindrical annulus using Lattice Boltzmann method, International Journal of Thermal Sciences 64 (2013) 240–250.

[32] M. Sheikholeslami, M. Gorji-Bandpy, K. Vajravelu, Lattice Boltzmann simulation of magneto-hydrodynamic natural convection heat transfer of Al_2O_3–water nanofluid in a horizontal cylindrical enclosure with an inner triangular cylinder, International Journal of Heat and Mass Transfer 80 (2015) 16–25.

[33] M. Sheikholeslami, M. Gorji-Bandpy, D.D. Ganji, S. Soleimani, Heat flux boundary condition for nanofluid filled enclosure in presence of magnetic field, Journal of Molecular Liquids 193 (2014) 174–184.

[34] F. Mebarek-Oudina, R. Bessaïh, Numerical simulation of natural convection heat transfer of copper-water nanofluid in a vertical cylindrical annulus with heat sources, Thermophysics and Aeromechanics 26 (3) (2019) 325–334.

[35] F. Mebarek-Oudina, A. Aissa, B. Mahanthesh, Hakan F.Öztop, Heat transport of magnetized Newtonian nanoliquids in an annular space between porous vertical cylinders with discrete heat source, International Communications in Heat and Mass Transfer 117 (2020), 104737.

[36] M.S. Sadeghi, Tahar Tayebi, A.S. Dogonchi, M.K. Nayak, M. Waqas, Analysis of thermal behavior of magnetic buoyancy-driven flow in ferrofluid–filled wavy enclosure furnished with two circular cylinders, International Communications in Heat and Mass Transfer 120 (2021), 104951.

[37] K. Khanafer, K. Vafai, A critical synthesis of thermophysical characteristics of nanofluids, International Journal of Heat and Mass Transfer 54 (19-20) (2011) 4410–4428.

[38] J.C. Maxwell, A Treatise on Electricity and Magnetism, second ed., Oxford University Press, Cambridge, 1904. pp. 435–441.

[39] C.H. Chon, K.D. Kihm, S.P. Lee, S.U.S. Choi, Empirical correlation finding the role of temperature and particle size for nanofluid (Al2O3) thermal conductivity enhancement, Applied Physics Letters 87 (15) (2005) 153107.

[40] K. Choukairy, R. Bennacer, H. Beji, S. Jaballah, M. El Ganaoui, Transient behavior inside a vertical cylindrical enclosure heated from the side walls, Numerical Heat Transfer, Part A, 50 (8) (2006) 773–785.

[41] Suhas V. Patankar, Numerical Heat Transfer and Fluid Flow, McGraw-Hill, 1980.

[42] H.C. Brinkman, The viscosity of concentrated suspensions and solutions, Journal of Chemical Physics 20 (4) (1952) 571–581.

[43] J. Maxwell, A treatise on electricity and magnetism, second ed., Oxford University Press, Cambridge, UK, 1904.

[44] S. P. Jang, S. U. S. Choi, The role of Brownian motion in the enhanced thermal conductivity of nanofluids, Applied Physics Letters 84 (2004)4316–4318.

[45] C. T. Nguyen, F. Desgranges, N. Galanis, G. Roy, T. Maré, S. Boucher, H. A. Mintsa, Viscosity data for Al_2O_3–water nanofluid—hysteresis: is heat transfer enhancement using nanofluids reliable? , International Journal of Thermal Sciences 47(2008) 103–111.

[46] E. Abu-Nada, Effects of variable viscosity and thermal conductivity of Al_2O_3–water nanofluid on heat transfer enhancement in natural convection, International Journal of Heat and Fluid Flow 30 (2009) 679–690.

[47] C. T. Nguyen, F. Desgranges, G. Roy, N. Galanis, T. Maré, S. Boucher, H. A. Minsta, Temperature and particle-size dependent viscosity data for water-based nanofluids – hysteresis phenomenon, International Journal of Heat and Fluid Flow 28 (2007) 1492–1506.

[48] C. H. Chon, K. D. Kihm, S. P. Lee, S. U. S. Choi, Empirical correlation finding the role of temperature and particle size for nanofluid (Al2O3) thermal conductivity enhancement, Applied Physics Letters 87 (2005) 153107.

[49] A. A. A. Arani, A. A. Azemati, M. Rezaee, B. S. Hadavand, Numerical study of different conduction models for Al_2O_3-water nanofluid with properties inside a trapezoidal enclosure, Journal of Mechanical Science and Technology 31 (5) (2017) 2433-2441.

[50] J. Koo, C. Kleinstreuer, Viscous dissipation effects in micro tubes and micro channels. International Journal of Heat and Mass Transfer 47 (2004) 3159-3169.

[51] M. Corcione, Empirical correlating equations for predicting the effective thermal conductivity and dynamic viscosity of nanofluids, Energy Conversion and Management 52 (2011) 789-793.

[52] J. Li, Computational analysis of nanofluid flow in micro channels with applications to micro-heat sinks and bio-MEMS, PhD Thesis. Raleigh, NC, the United States : North Carolina State University; 2008.

[53] B. V. K. Satya Sai, K. N. Seetharamu, P. A. Aswatha Narayana, J. N. Reddy, Finite element analysis of the effect of radius ratio on natural convection in an annular cavity, International Journal of Numerical Method for Heat Fluid Flow 3 (4) (1993) 305–318.

[54] W. S. Yeung, Analysis of natural convection in a closed vertical annulus, International Communications in Heat and Mass Transfer 16 (3) (1989) 445–455.

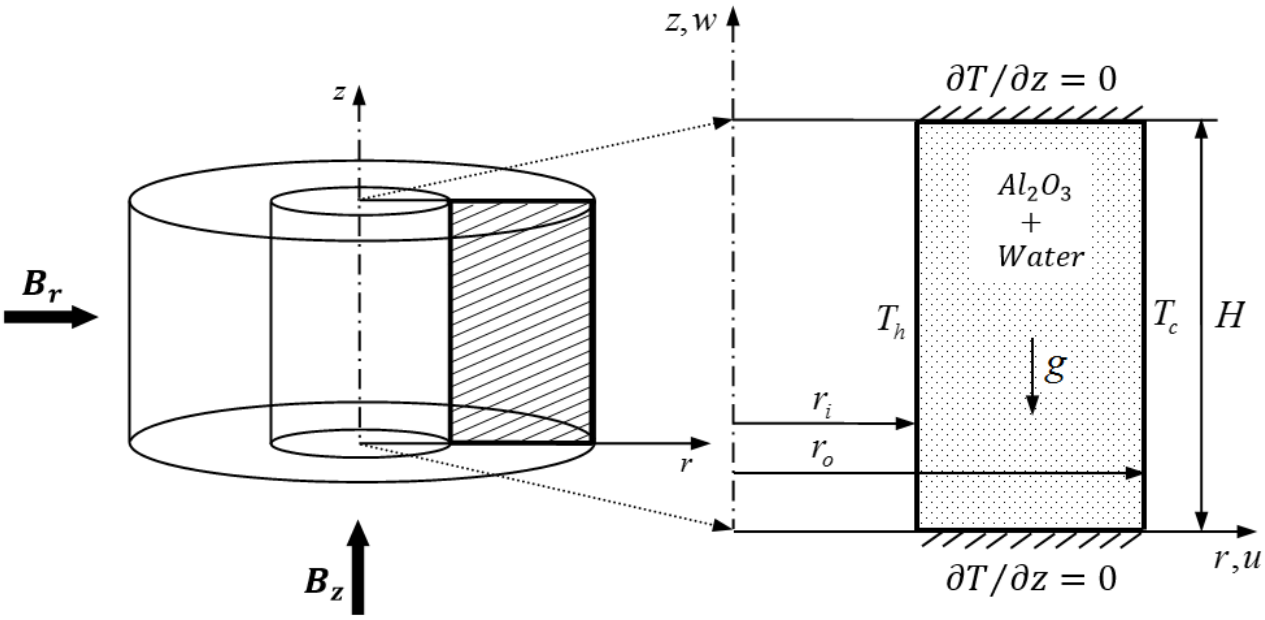

Fig. 1. Schematic of the problem.

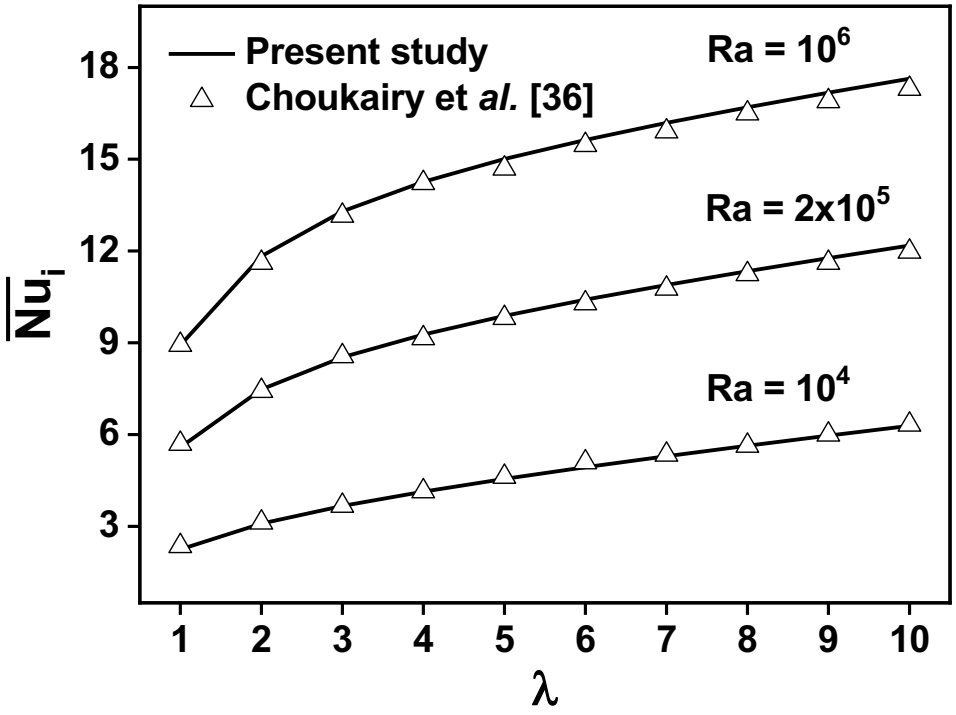

Fig. 2. Comparison of $\overline{Nu}_i$ numbers with [36].

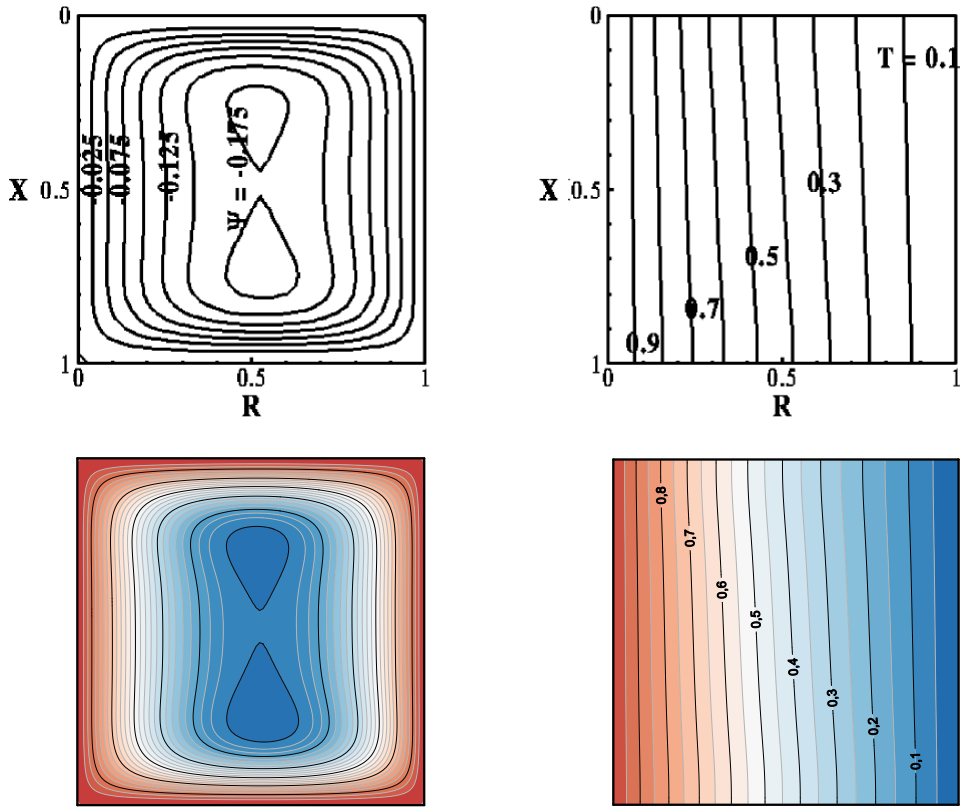
0
X 0.5
1
0
0.5
1
R
-0.025
-0.075
-0.125
Ψ = -0.175
T = 0.1
0.3
0.5
0.7
0.9
0.8
0.7
0.6
0.5
0.4
0.3
0.2
0.1

(a)

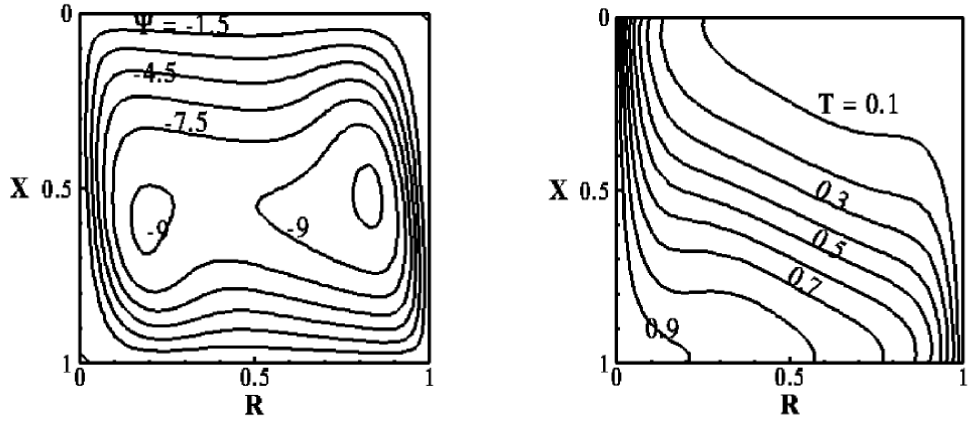
0
X 0.5
1
0
0.5
1
R
Ψ = -1.5
-4.5
-7.5
-9
-9
T = 0.1
0.3
0.5
0.7
0.9

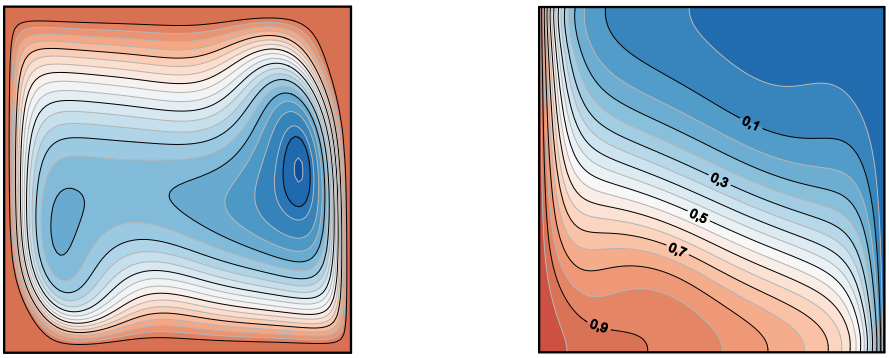

(b)

Fig. 3. Comparison of streamlines and isotherms with [14] for Pr = 0.054, A =1 and $\lambda = 2$ at (a) $Ra = 10^4$, $Ha = 100$ (radial magnetic field) and (b) $Ra = 10^6$, $Ha = 100$ (axial magnetic field).

ψ

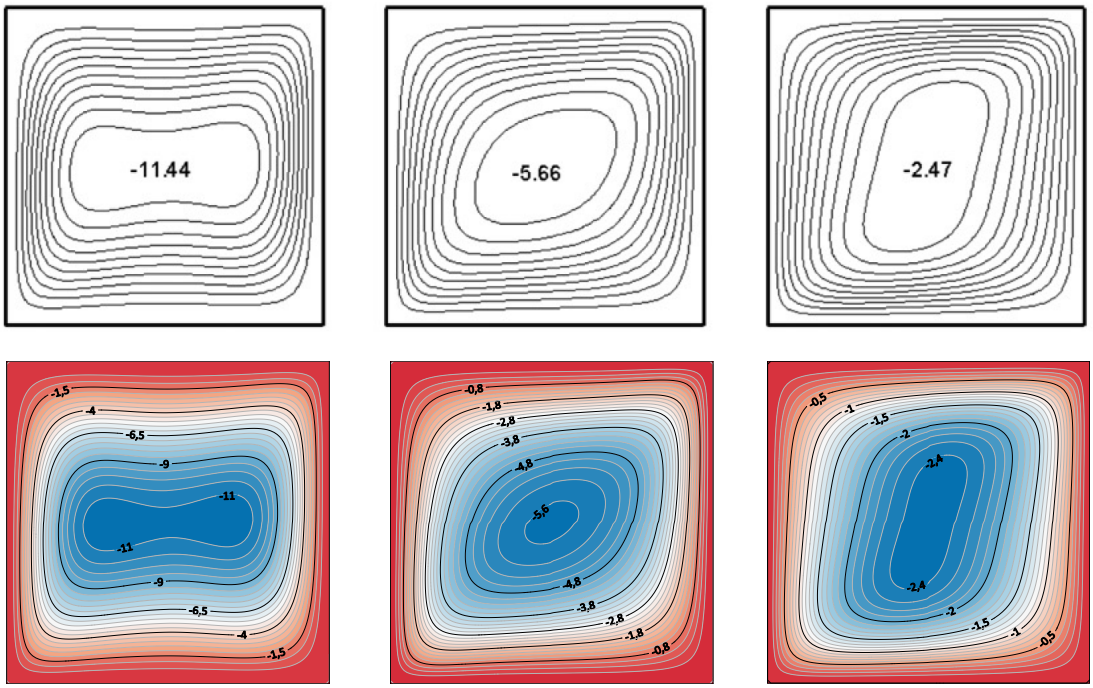

$|\psi_f|_{max} = 11.427$ $|\psi_f|_{max} = 5.662$ $|\psi_f|_{max} = 2.465$

θ

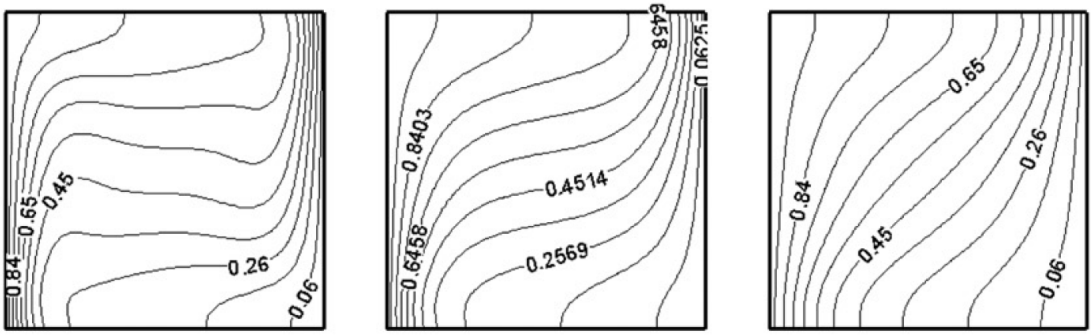

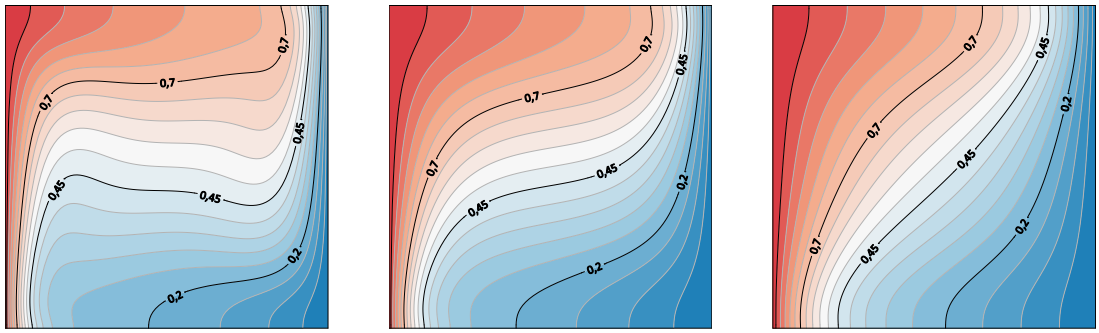

(a) **(b)** **(c)**

Fig. 4. Comparison of streamlines and isotherms with [26] for $Ra = 10^6$ and $\varphi = 0.03$ at (a) $Ha = 0$, (b) $Ha = 30$, and (c) $Ha = 60$ (horizontal magnetic field).

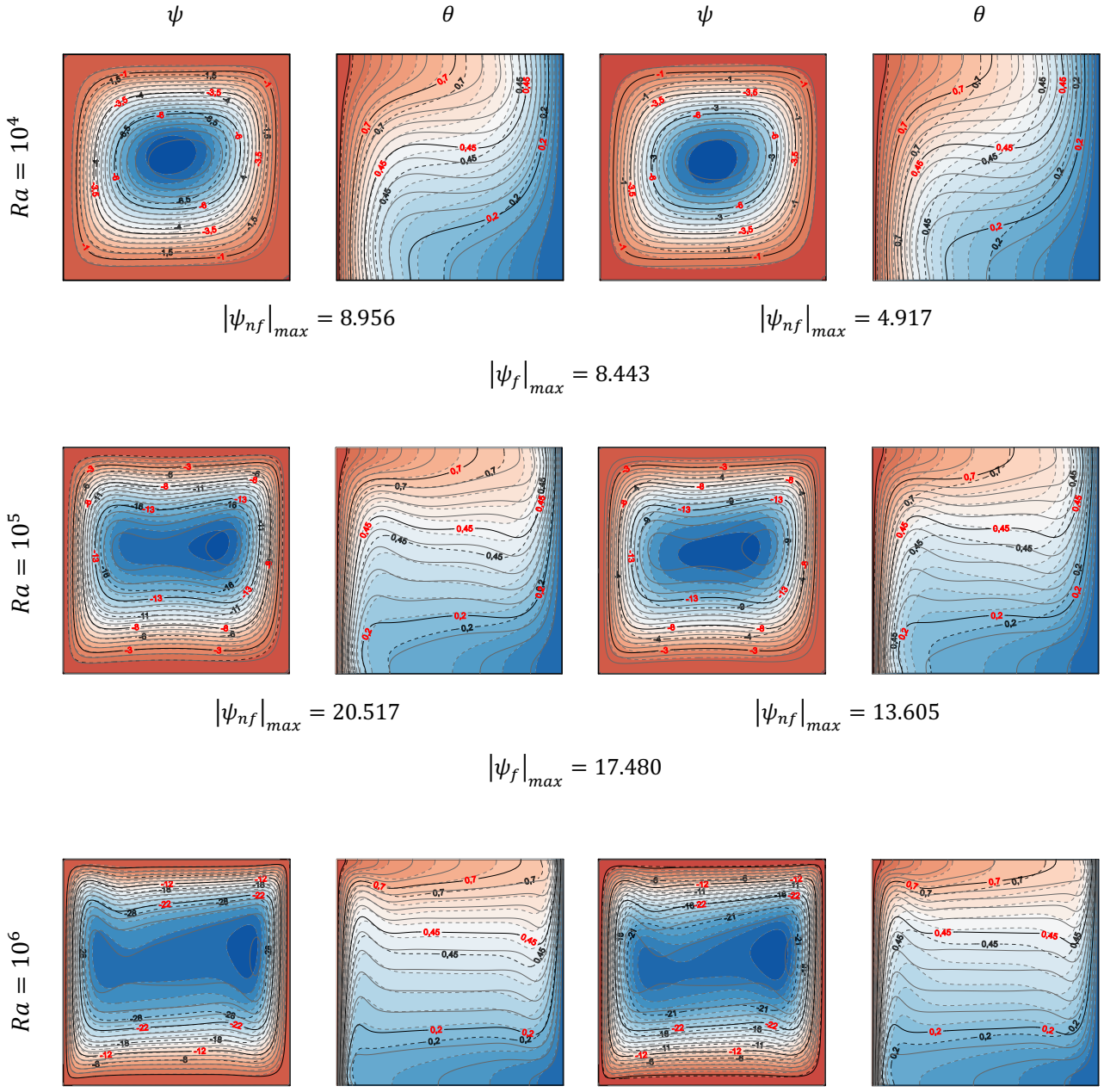

$|\psi_{nf}|_{max} = 37.357$ $|\psi_{nf}|_{max} = 25.980$

$|\psi_f|_{max} = 30.314$

(a) **(b)**

Fig. 5. Streamline (left) and isotherm (right) contours for $\varphi = 0$ (solid lines) and $\varphi = 0.09$ (dashed lines) at $Ra = 10^6$ and $= 2$: (a) $d_p = 13\ nm$, (b) $47\ nm$.

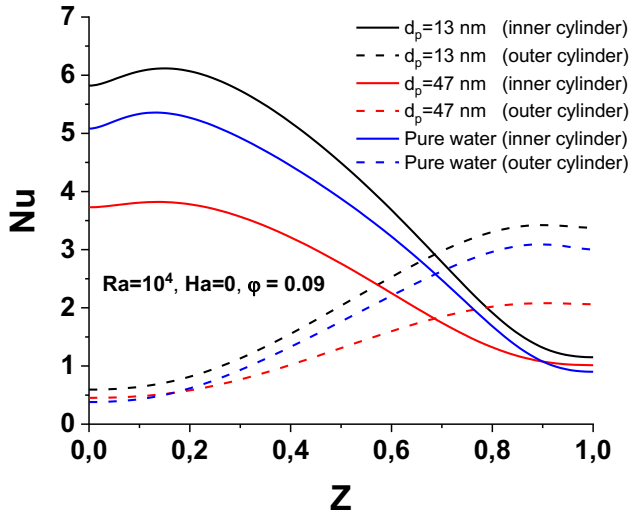

(a)

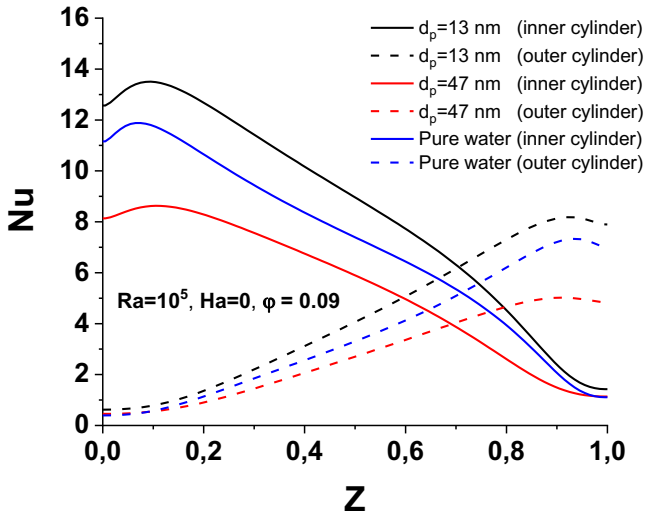

(b)

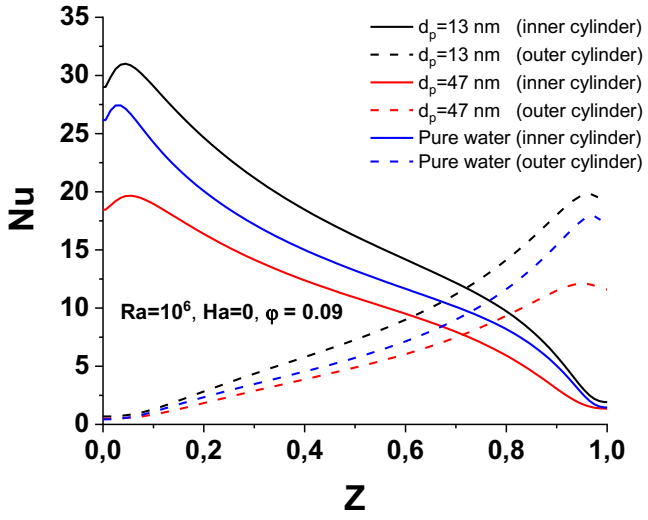

(c)

Fig. 6. Variation of Nu along the surface of the inner and outer cylinder for different Ra.

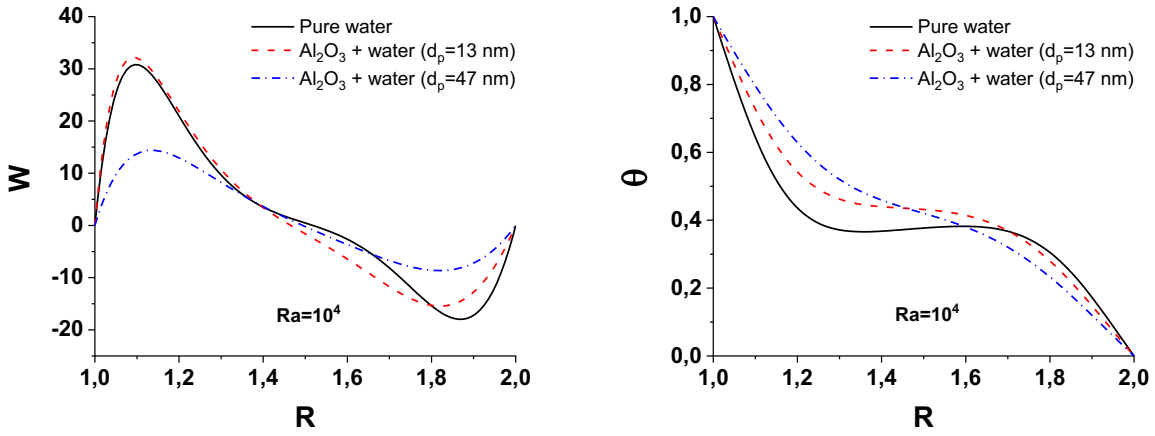

(a)

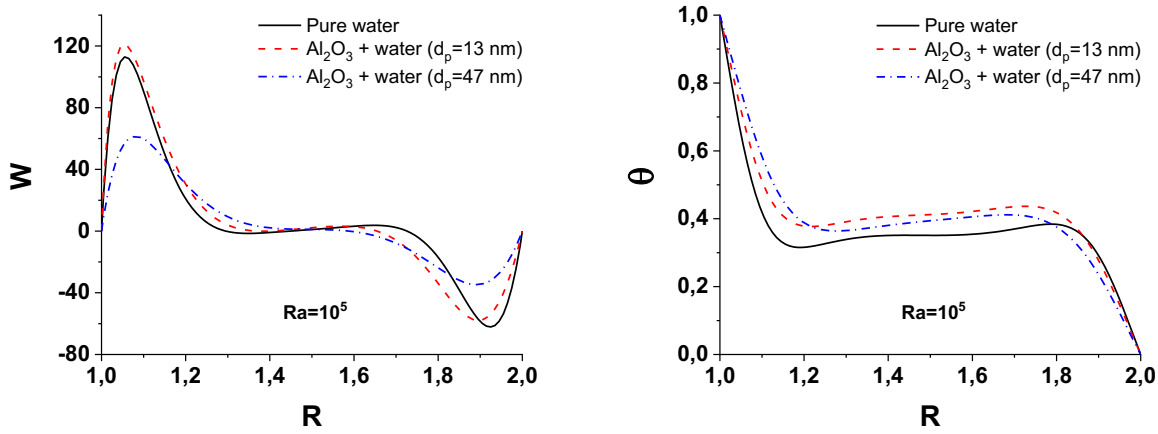

(b)

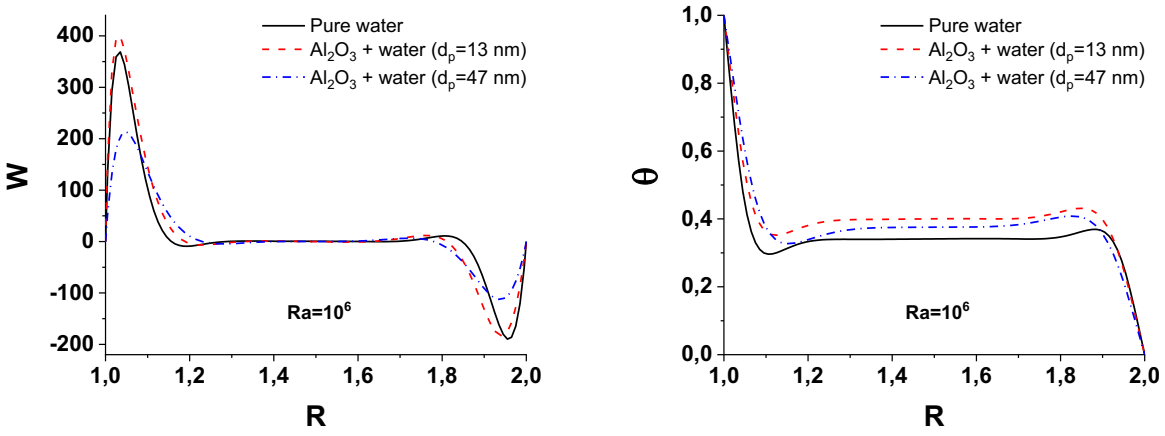

(c)

Fig. 7. Variation of axial velocity U (left) and temperature θ (right) at half height along R direction for different Ra at $\lambda = 2$: $\varphi = 0$ (pure water) and $\varphi = 0.09$ (nanofluid $d_p = 13$ and $47\ nm$).

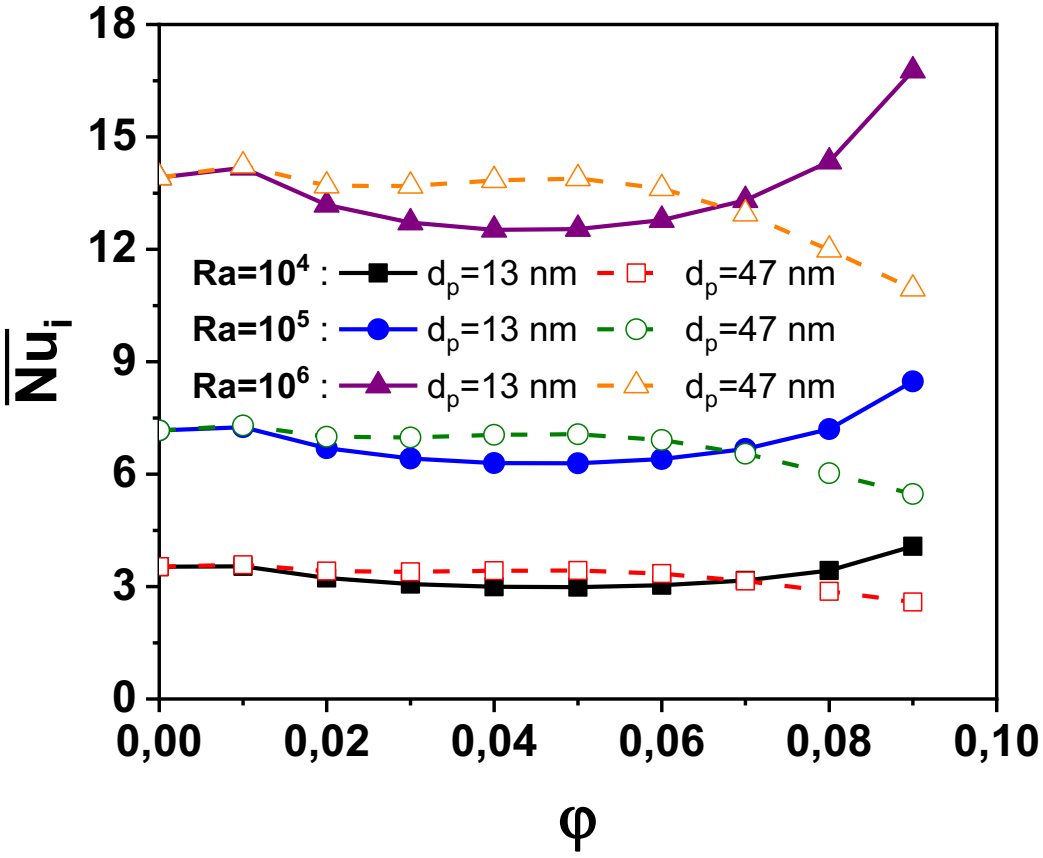

Fig. 8. Variation of $\overline{Nu_i}$ with φ for different Ra at $\lambda = 2$.

ψ

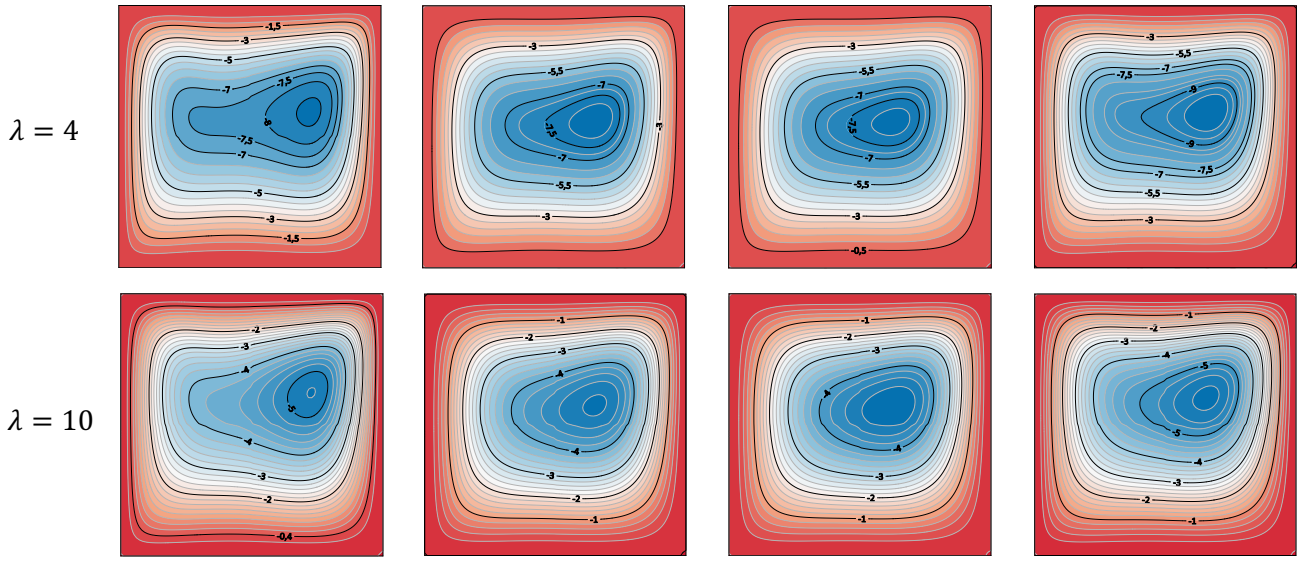

(a) $Ra = 10^5$

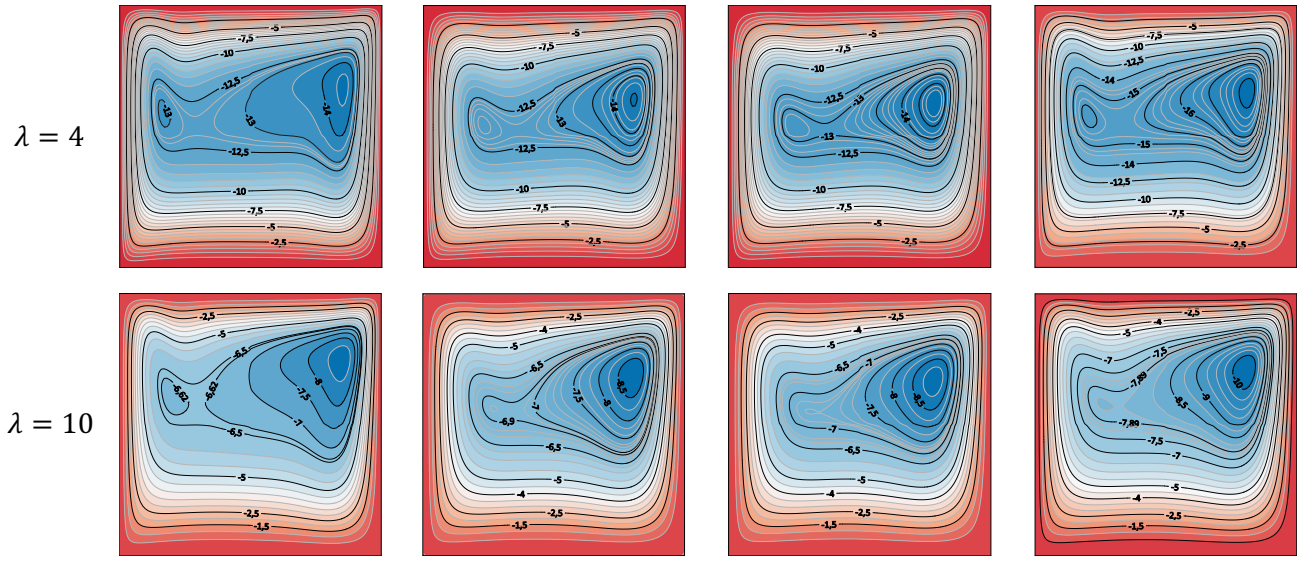

(b) $Ra = 10^6$

θ

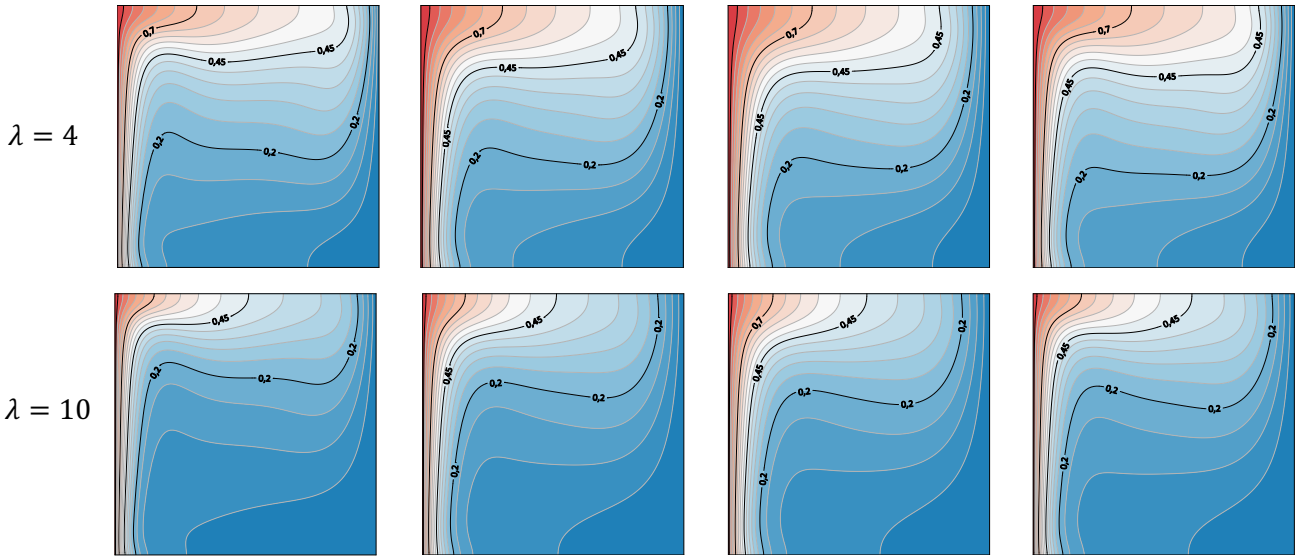

(a) $Ra = 10^5$

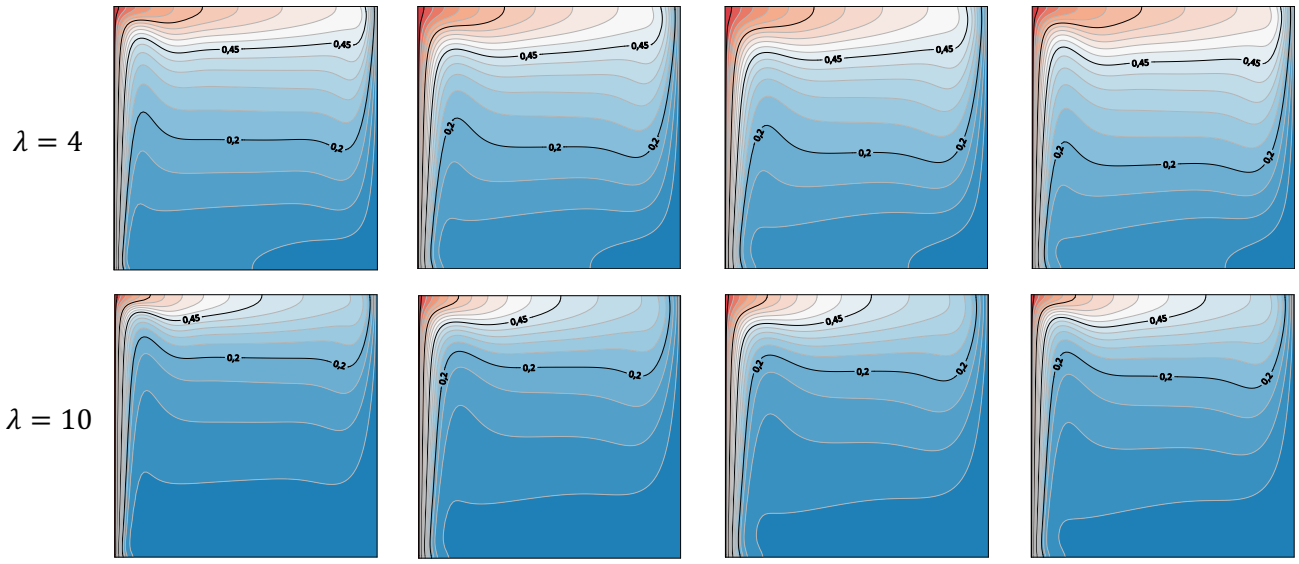

(b) $Ra = 10^6$

Fig. 9. Streamlines and isotherms for $d_p = 13\ nm$, $Ra = 10^5$, 10^6 and $\lambda = 2$, 10 at different φ.

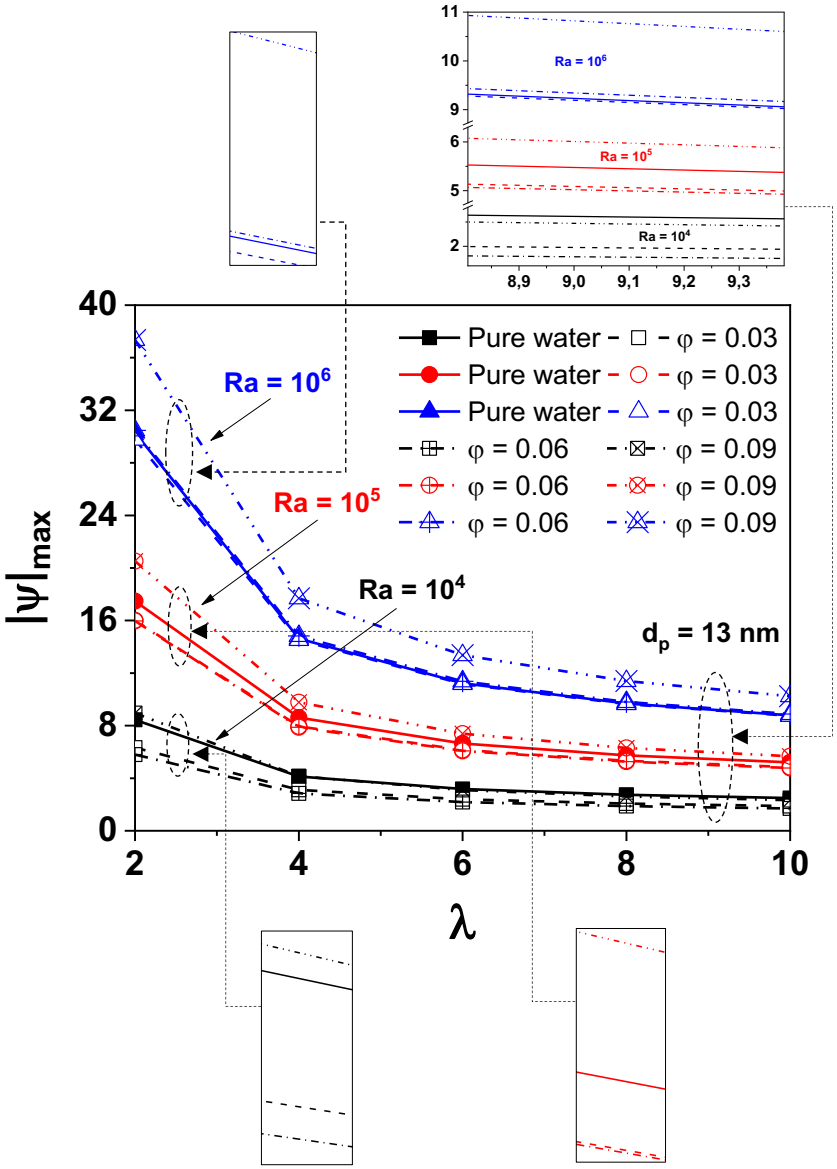

Fig. 10. Effect of λ on the maximum stream function $|\psi|_{max}$ for different Ra and φ at $d_p = 13\ nm$.

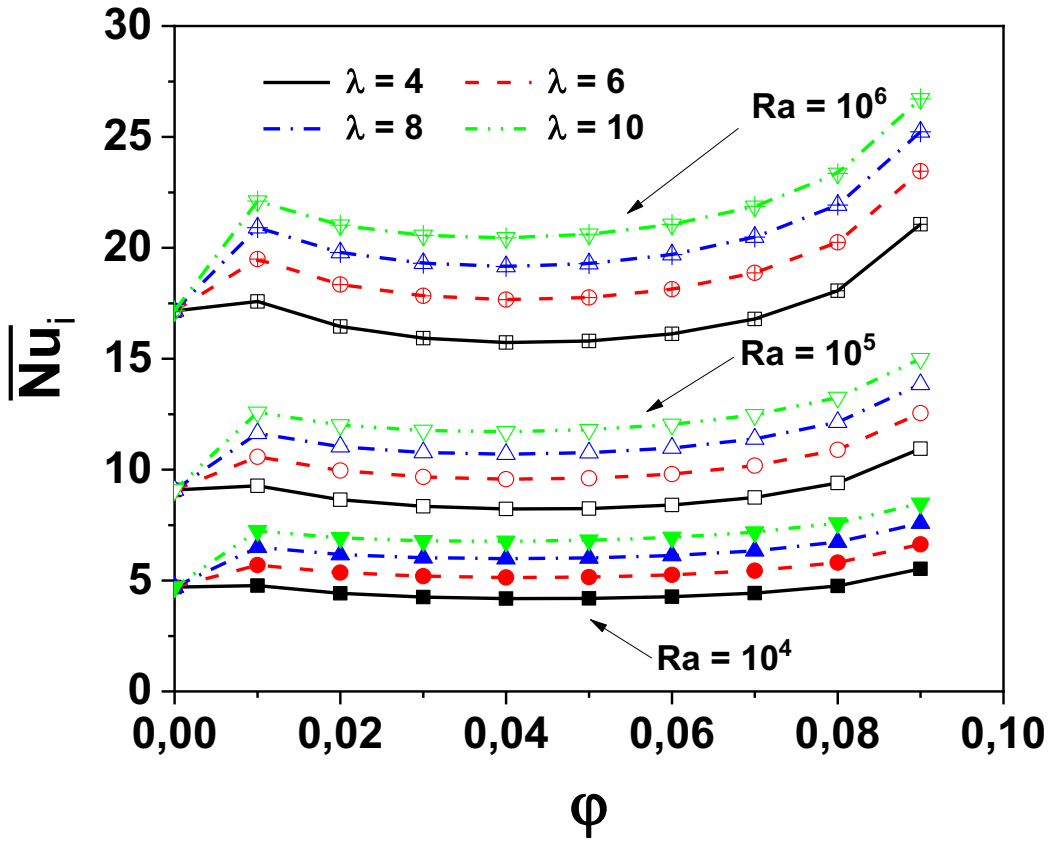

Fig. 11. Variation of $\overline{Nu}_i$ with φ for different Ra and λ at $d_p = 13\ nm$.

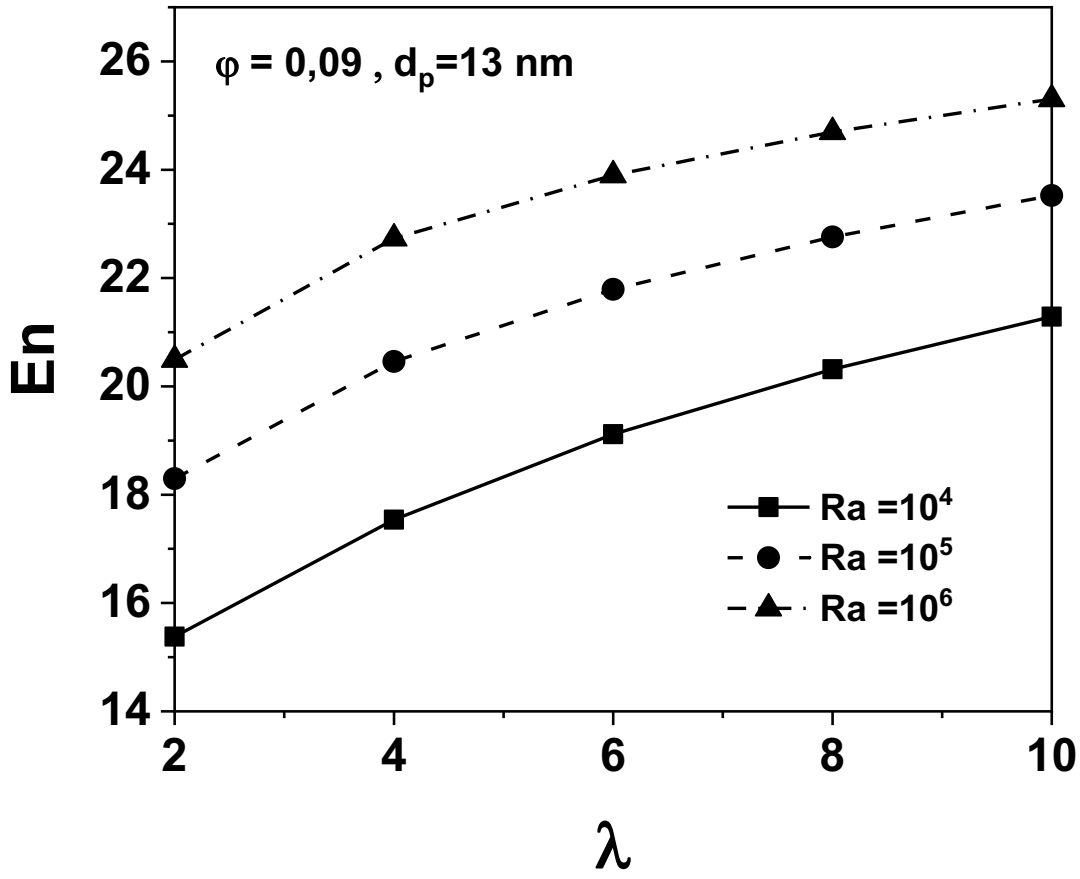

Fig. 12. Effects of Ra and λ on the heat transfer enhancement ratio En for $\varphi = 0.09$ and $d_p = 13\ nm$.

Radial magnetic field, B_r

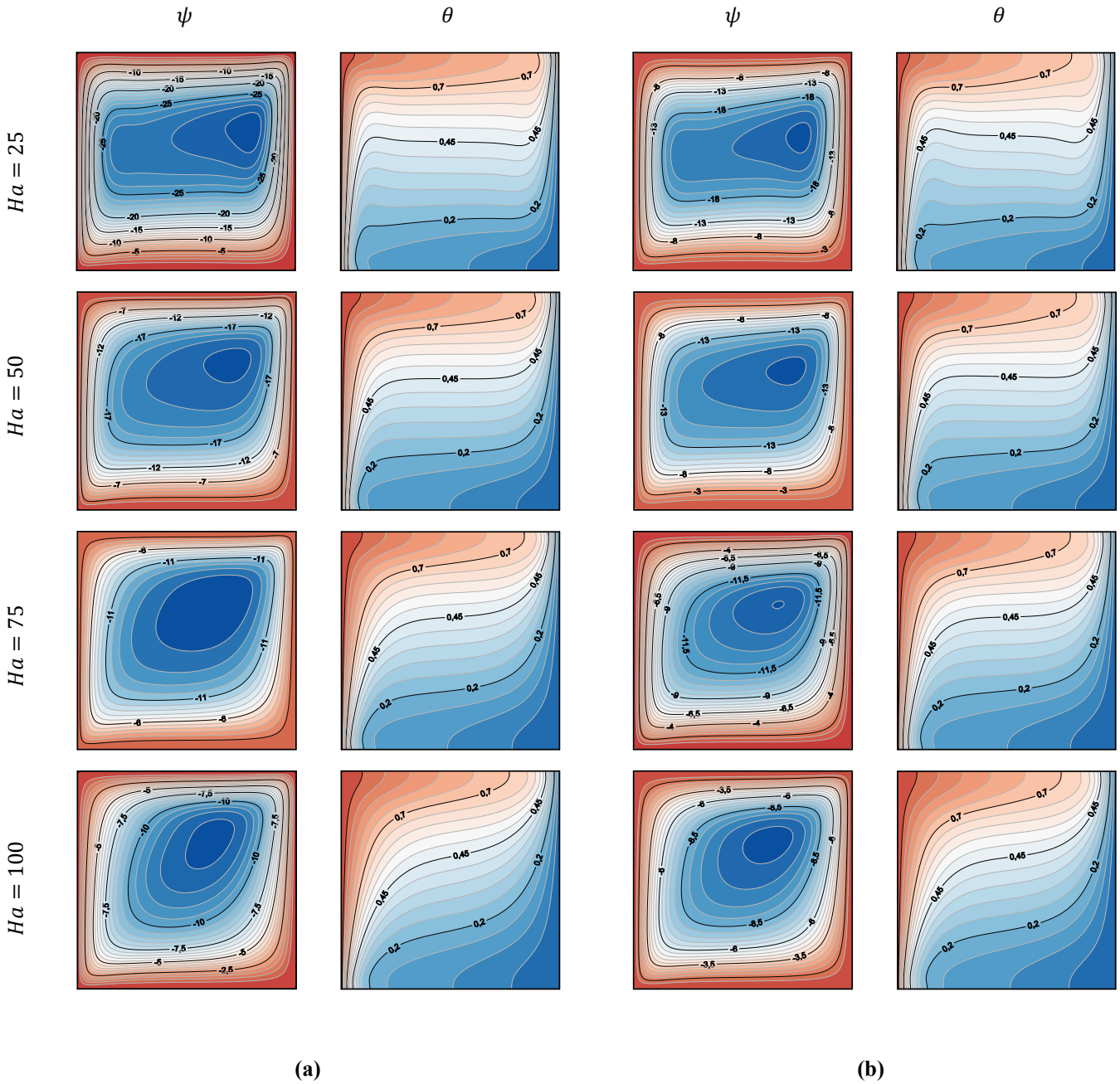

Axial magnetic field, B_z

ψ θ ψ θ

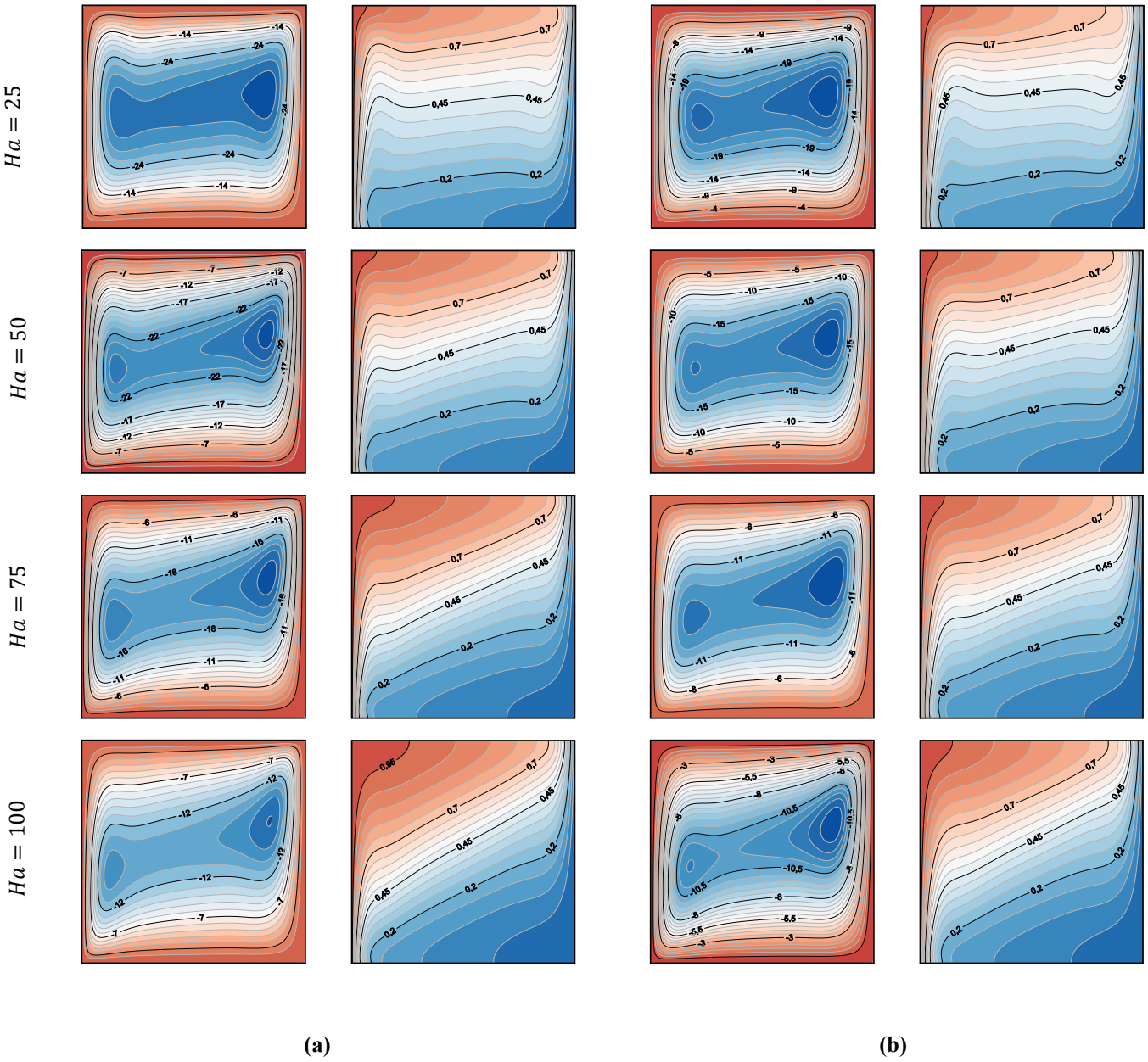

Fig. 13. Effect of Ha on streamlines (left) and isotherms (right) for $Ra = 10^6$and $\varphi = 0.09$ at (a) $d_p = 13\ nm$ and (b) $47\ nm$.

$$\boldsymbol{Ra = 10^4}$$

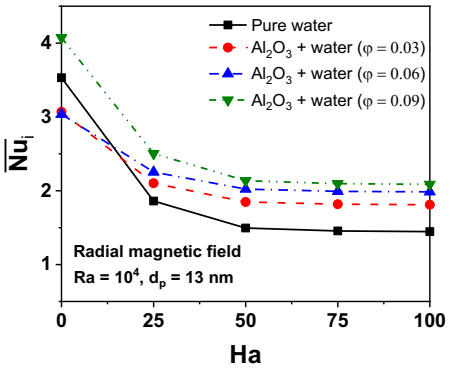
Pure water
Al2O3 + water (φ = 0.03)
Al2O3 + water (φ = 0.06)
Al2O3 + water (φ = 0.09)
Radial magnetic field
Ra = 10^4, dp = 13 nm
Nui
Ha

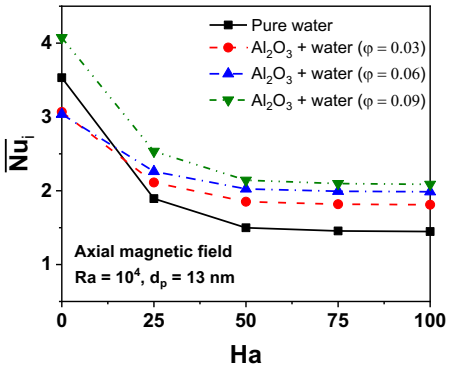
Pure water
Al2O3 + water (φ = 0.03)
Al2O3 + water (φ = 0.06)
Al2O3 + water (φ = 0.09)
Axial magnetic field
Ra = 10^4, dp = 13 nm
Nui
Ha

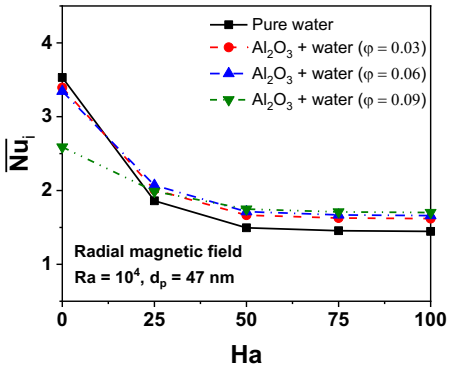
Pure water
Al2O3 + water (φ = 0.03)
Al2O3 + water (φ = 0.06)
Al2O3 + water (φ = 0.09)
Radial magnetic field
Ra = 10^4, dp = 47 nm
Nui
Ha

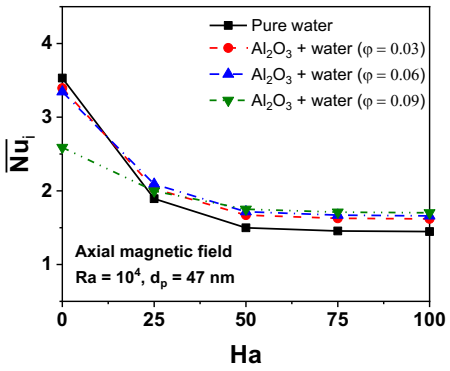
Pure water
Al2O3 + water (φ = 0.03)
Al2O3 + water (φ = 0.06)
Al2O3 + water (φ = 0.09)
Axial magnetic field
Ra = 10^4, dp = 47 nm
Nui
Ha

$$Ra = 10^5$$

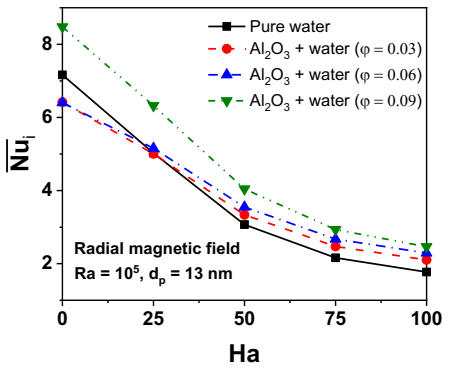
Pure water
Al2O3 + water (φ = 0.03)
Al2O3 + water (φ = 0.06)
Al2O3 + water (φ = 0.09)
Radial magnetic field
Ra = 10^5, dp = 13 nm
Nui
Ha

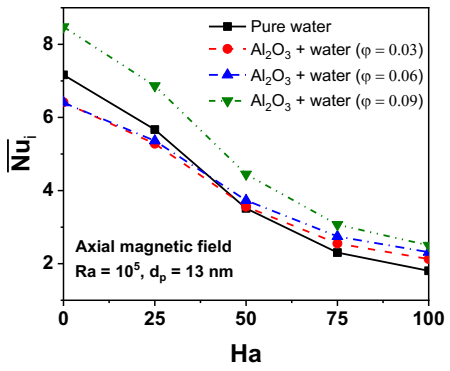
Pure water
Al2O3 + water (φ = 0.03)
Al2O3 + water (φ = 0.06)
Al2O3 + water (φ = 0.09)
Axial magnetic field
Ra = 10^5, dp = 13 nm
Nui
Ha

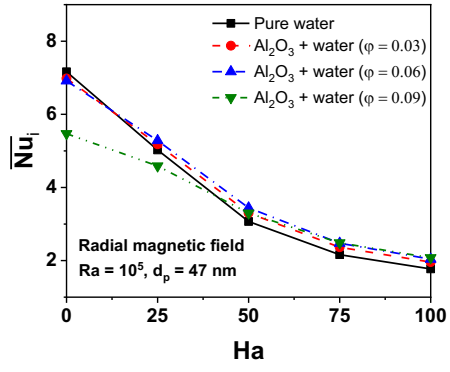
Pure water
Al2O3 + water (φ = 0.03)
Al2O3 + water (φ = 0.06)
Al2O3 + water (φ = 0.09)
Radial magnetic field
Ra = 10^5, dp = 47 nm
Nui
Ha

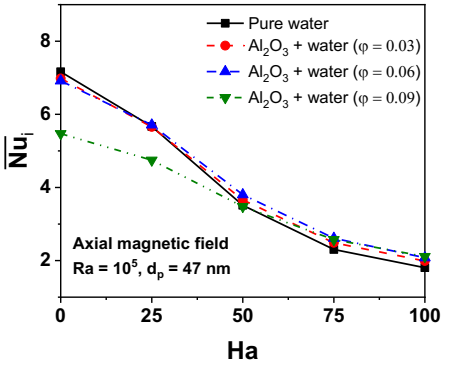
Pure water
Al2O3 + water (φ = 0.03)
Al2O3 + water (φ = 0.06)
Al2O3 + water (φ = 0.09)
Axial magnetic field
Ra = 10^5, dp = 47 nm
Nui
Ha

$$Ra = 10^6$$

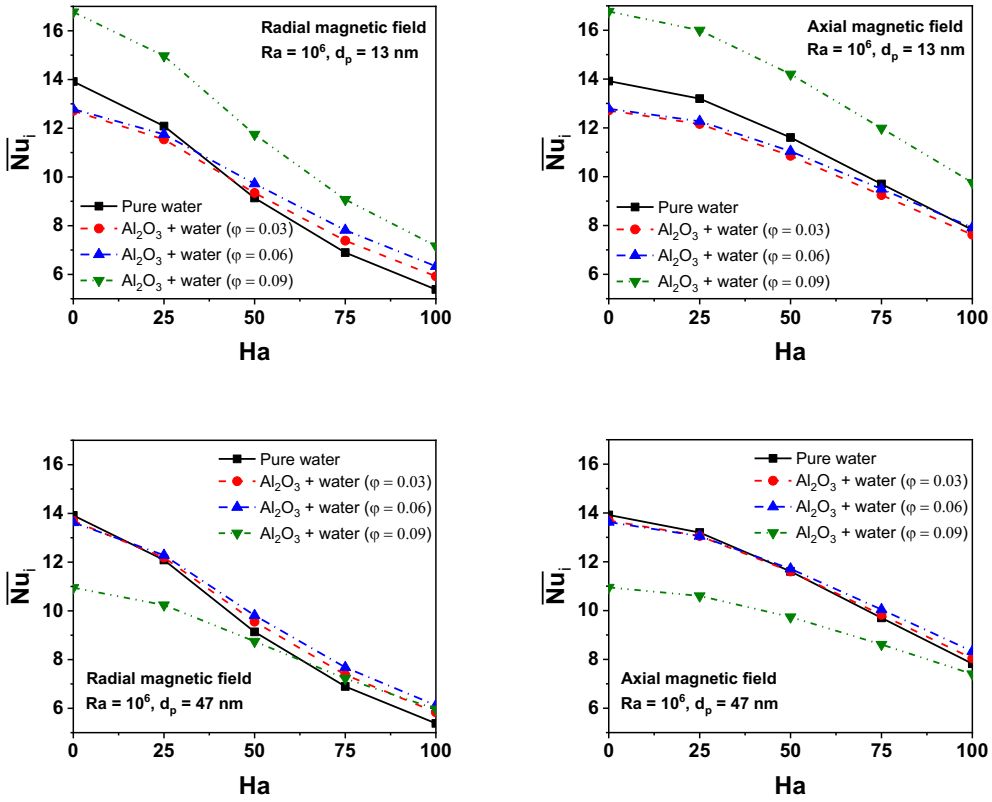

Fig. 14. Effect of Ha on the average $\overline{Nu}_i$ for different Ra and φ at $\lambda = 2$ and $d_p = 13\ nm$, $47\ nm$: (a) B_r and (b) B_z.

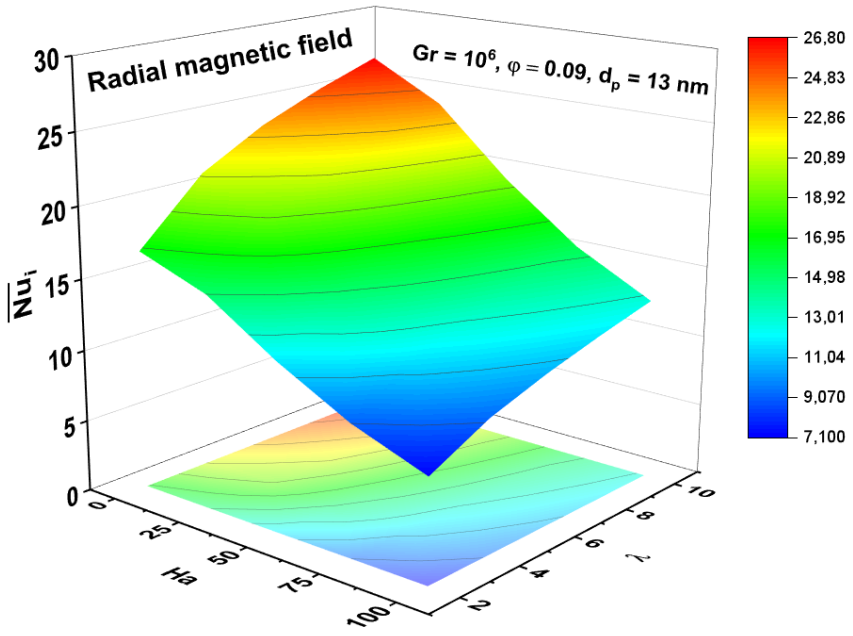

(a)

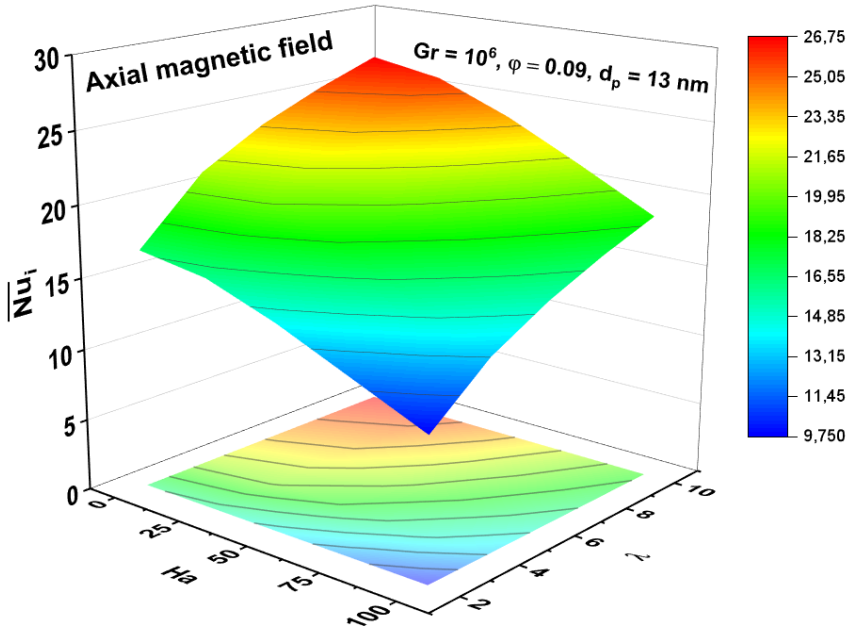

(b)

Fig. 15. Effects of Ha and λ on the average $\overline{Nu_i}$ for $Ra = 10^6$, $\varphi = 0.09$ and $d_p = 13\ nm$: (a) B_r and (b) B_z.

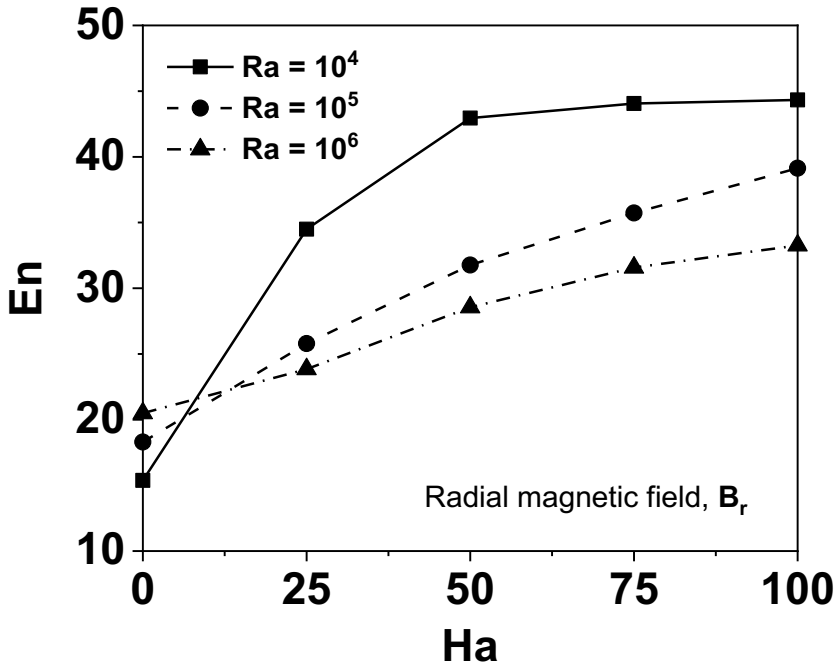

(a)

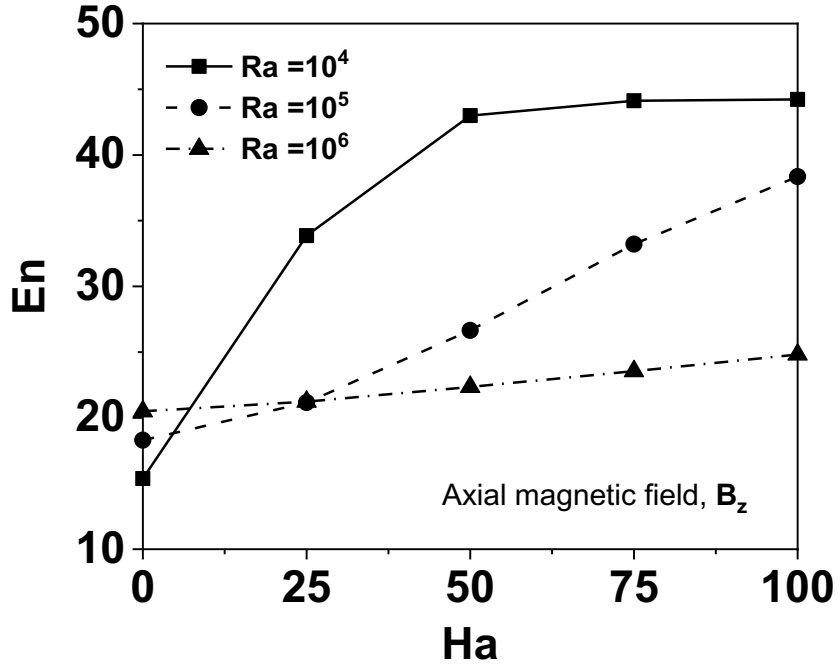

(b)

Fig. 16. Effects of Ra and Ha on the heat transfer enhancement ratio En for $\varphi = 0.09$ and $d_p = 13\ nm$: (a) B_r and (b) B_z.

Table 1. Thermo-physical properties of water and alumina [27].

	Pr	$\boldsymbol{\rho\ (kg/m^3)}$	$\boldsymbol{c_p(J/kgK)}$	$\boldsymbol{k\ (W/mK)}$	$\boldsymbol{\beta \times 10^{-5}\ (1/K)}$	$\boldsymbol{\sigma\ (1/\Omega.m)}$
Pure water	6.2	997.1	4179	0.613	21	0.05
Alumina $\boldsymbol{(Al_2O_3)}$		3970	765	40	0.85	10^{-5}

Table 2. Characteristics of the flow for different grids at: $Ra = 10^5$, Pr $= 6.2$, $Ha = 50$, $\varphi = 0.06$ and $dp = 13\ nm$.

$\boldsymbol{Grid}$	$\boldsymbol{52 \times 52\ nodes}$	$\boldsymbol{102 \times 102\ nodes}$	$\boldsymbol{202 \times 202\ nodes}$
$\boldsymbol{\overline{Nu}_i}$	3.574	3.550	3.542
$\boldsymbol{U_{max}}$	17.528	17.490	17.490
$\boldsymbol{W_{max}}$	21.563	21.649	21.651
$\boldsymbol{\lvert\psi\rvert_{max}}$	5.896	5.887	5.889

Table 3. Comparison of $\overline{Nu}_i$ with [26] for different Ra and φ at $Ha = 30$.

	$\varphi = 0$	$\varphi = 0.02$	$\varphi = 0.04$	$\varphi = 0.06$
$\boldsymbol{Ra = 10^3}$				
Ghasemi et al.[26]	1.002	1.060	1.121	1.184
Present work	1.002	1.060	1.120	1.183
$\boldsymbol{Ra = 10^4}$				
Ghasemi et al.[26]	1.183	1.212	1.249	1.291
Present work	1.182	1.212	1.248	1.290
$\boldsymbol{Ra = 10^5}$				
Ghasemi et al.[26]	3.150	3.138	3.124	3.108
Present work	3.149	3.137	3.123	3.107
$\boldsymbol{Ra = 10^6}$				
Ghasemi et al.[26]	7.907	7.979	8.042	8.098
Present work	7.907	7.978	8.042	8.097
$\boldsymbol{Ra = 10^7}$				
Ghasemi et al.[26]	16.929	17.197	17.449	17.688
Present work	16.926	17.194	17.447	17.687

Table 4. Natural convection of nanofluid in cylinder/annulus enclosure with and without applied magnetic field

Authors	Method	NF	Case study	Magnitic field	Parameters	Models	Conclusions
Abouali and Falahatpisheh [27]	FVM	Al_2O_3	Natural convection in vertical annuli differentially heated	/	$d_p = 36\ nm$ $1 \leq A = \frac{H}{r_o - r_i} \leq 5$ $10^3 \leq Gr \leq 10^5$ $0 \leq \varphi \leq 0.06$	K_{nf} : model of Jang and Choi [44] μ_{nf}: model of Nguyen et al. [45]	- $\overline{Nu}$ decreases with the increase of φ independently of the Grashof number, the aspect ratio ($A \geq 1$) and the radius ratio of the ring following the correlation: $\overline{Nu} = \overline{Nu}_f(1 - c\varphi)$ where the constant c depends on the particle diameter dp and how the viscosity μ_{nf} varies with φ. - The model of Jang and Choi (K_{nf}) agrees with the experience of Putra et al. [26] and shows a deterioration in heat transfer.
Abu-Nada [46]	FVM	Al_2O_3	Natural convection in horizontal annuli	/	$d_p = 47\ nm$ $0.2 \leq \frac{r_o - r_i}{r_i} \leq 0.8$ $10^3 \leq Ra \leq 10^5$ $0 \leq \varphi \leq 0.09$	K_{nf}: 1. model of Chon et al. [47] 2. model of Maxwell-Garnett [43] μ_{nf}: 1. Model of Nguyen et al. [48] 2. Model of Brinkman [42]	- For $Ra \geq 10^4$ and $\varphi > 0.05$, $\overline{Nu}$ is reduced by increasing φ. - at $Ra = 10^3$, $\overline{Nu}$ increases with increasing φ. - For $Ra \geq 10^4$, the difference between the prediction of MG and that of the model of Chon et al. is weak. However, there is a deviation at $Ra = 10^3$ and this deviation becomes more significant at high \ varphi. - The Nguyen and Brinkman models give completely different predictions for $Ra \geq 10^4$ where the difference of $\overline{Nu}$ exceeds 30%. However, this difference reduces to less than 10% at $Ra = 10^3$.
Sheikholeslami et al. [29]	LBM	Al_2O_3	MHD Natural convection in a concentric annulus between a cold square and heated elliptic cylinders	/	$d_p = 47\ nm$ $10^4 \leq Ra \leq 10^6$ $0 \leq Ha \leq 100$ $0 \leq \varphi \leq 0.04$	K_{nf} and μ_{nf}: Correlation of Koo-Kleinstreuer- Li [50,52]	- $\overline{Nu}$ is an increasing function of φ and Ra, while it is a decreasing function of Ha.
Ashorynejad et al. [31]	LBM	Ag	MHD Natural convection heat transfer in a horizontal cylindrical annulus enclosure	Radial magnetic field	$\frac{r_o}{r_i} = 3$ $10^3 \leq Ra \leq 10^5$ $0 \leq Ha \leq 60$ $0 \leq \varphi \leq 0.06$	K_{nf}: Model of Maxwell-Garnett [43] μ_{nf}: Model of Brinkman [42]	- $\overline{Nu}$ is an increasing function of φ and Ra, while it is a decreasing function of Ha. - $\lvert\psi_{nf}\rvert_{max}$ increases as φ increases or Ra increases, while it decreases as Ha increases.

Sheikholeslami et al. [32]	LBM	Al_2O_3	MHD natural convection in a horizontal annulus with heated triangular inner cylinder and couled outer circular cylinder	Horizontal magnetic field	$d_p = 47\ nm$ $10^3 \leq Ra \leq 10^5$ $0 \leq Ha \leq 100$ $0 \leq \varphi \leq 0.04$	K_{nf} and μ_{nf}: Correlation of Koo-Kleinstreuer- Li [50,52]	- $\overline{Nu}$ is an increasing function of Ra, while it is a decreasing function of Ha. - $\lvert\psi_{nf}\rvert_{max}$ decreases as Ha increases.
Sheikholeslami et al. [33]	CVFEM	Al_2O_3	MHD natural convection in a horizontal annulus with cold outer cylinder, and the inner circular wall is under constant heat flux	Horizontal magnetic field	$d_p = 47\ nm$ $0.2 \leq \frac{r_{in}}{L} \leq 0.4$ $10^3 \leq Ra \leq 10^5$ $0 \leq Ha \leq 100$ $0 \leq \varphi \leq 0.04$	K_{nf} and μ_{nf}: Correlation of Koo-Kleinstreuer- Li [50,52]	$\overline{Nu}$ is an increasing function of φ, Ra, and of the aspect ratio ($\frac{r_{in}}{L}$) while it is a decreasing function of Ha
Present work	FVM	Al_2O_3	MHD natural convection in vertical annuli differentially heated	Radial and horizontal magnetic fields	$d_p = 13$ and $47\ nm$ $2 \leq \lambda = \frac{r_o}{r_i} \leq 10$ $10^4 \leq Ra \leq 10^6$ $0 \leq Ha \leq 100$ $0 \leq \varphi \leq 0.09$	K_{nf} and μ_{nf}: Correlation of Khanafer and Vafai [37]	- $\overline{Nu}$ is an increasing function of Ra, and of the radius ratio λ while it is a decreasing function of Ha. - For $\lambda = 2$, $\overline{Nu}$ is a decreasing function of φ for $d_p = 47\ nm$. - For $d_p = 13\ nm$ and $\lambda = 2$ and 4, $\overline{Nu}$ decreases to $\varphi = 0.05$ and then increases to its maximum at $\varphi = 0.09$. - For $d_p = 13\ nm$ and $\lambda \geq 6$, the heat transfer rate of the nanofluid is greater than that of the base fluid for all values of φ. - The influence of the magnetic field is more pronounced in the radial direction. - With the magnetic field, the rate of decrease in $\overline{Nu}$ is greater as λ decreases. - As Ra, Ha and λ are increased, the heat transfer enhancement ratio En increases and for high values of Ha, En increases further at the expense of Ra.

Table 5. Effect of Ha on the characteristics of the flow for different Ra at $\varphi = 0.09$ and $d_p = 13\ nm$.

		$Ha = 0$	$Ha = 25$		$Ha = 50$		$Ha = 75$		$Ha = 100$	
			$\boldsymbol{B_r}$	$\boldsymbol{B_z}$	$\boldsymbol{B_r}$	$\boldsymbol{B_z}$	$\boldsymbol{B_r}$	$\boldsymbol{B_z}$	$\boldsymbol{B_r}$	$\boldsymbol{B_z}$
	$\boldsymbol{U_{max}}$	22.804	7.779	7.296	3.099	2.562	1.737	1.241	1.141	0.729
$Ra = 10^4$	$\boldsymbol{W_{max}}$	32.245	9.349	12.518	2.790	5.030	1.300	2.836	0.747	1.883
	$\boldsymbol{\|\psi\|_{max}}$	8.956	2.907	2.877	0.886	0.904	0.409	0.425	0.234	0.246
	$\boldsymbol{U_{max}}$	66.697	37.912	35.515	23.659	23.276	15.847	13.743	11.151	8.219
$Ra = 10^5$	$\boldsymbol{W_{max}}$	122.369	66.780	88.579	28.391	52.932	14.075	31.409	8.069	20.204
	$\boldsymbol{\|\psi\|_{max}}$	20.517	12.659	12.781	6.596	6.904	3.700	3.915	2.276	2.399
	$\boldsymbol{U_{max}}$	190.033	127.715	125.880	91.429	90.477	72.371	78.542	59.301	67.020
$Ra = 10^6$	$\boldsymbol{W_{max}}$	406.671	311.433	375.323	198.026	317.074	123.813	262.889	80.495	214.288
	$\boldsymbol{\|\psi\|_{max}}$	37.357	29.649	33.479	21.347	26.491	15.953	20.596	12.230	16.050